Interpretation of Volume and Flux Changes of the Laurichard Rock Glacier Between 1952 and 2019, French Alps

Diego Cusicanqui, Antoine Rabatel, Christian Vincent, Xavier Bodin, Emmanuel Thibert, Bernard Francou

JGR Earth Surface

RESEARCH ARTICLE
10.1029/2021JF006161

Interpretation of Volume and Flux Changes of the Laurichard Rock Glacier Between 1952 and 2019, French Alps

Diego Cusicanqui[1,2], Antoine Rabatel[1], Christian Vincent[1], Xavier Bodin[2], Emmanuel Thibert[3], and Bernard Francou[1]

[1]Université Grenoble Alpes, CNRS, IRD, Institut de Géosciences de l'Environnement (IGE, UMR 5001), Grenoble, France, [2]Laboratoire EDYTEM, Université Savoie Mont-Blanc, CNRS, Le Bourget du Lac, France, [3]Université Grenoble Alpes, INRAE, UR ETGR, Saint-Martin-d'Hères, France

Key Points:

- We used historical and modern aerial images to document changes in thickness, flow velocities, and the ice/rock flux of the rock glacier
- This is the first time that emergence velocities and the surface mass balances have been reconstructed for a rock glacier
- Strong marked acceleration of the entire rock glacier after 1990s, likely a consequence of changes in the basal conditions

Supporting Information:

Supporting Information may be found in the online version of this article.

Correspondence to:

D. Cusicanqui,
diego.cusicanqui@univ-grenoble-alpes.fr

Citation:

Cusicanqui, D., Rabatel, A., Vincent, C., Bodin, X., Thibert, E., & Francou, B. (2021). Interpretation of volume and flux changes of the Laurichard rock glacier between 1952 and 2019, French Alps. *Journal of Geophysical Research: Earth Surface*, *126*, e2021JF006161. https://doi.org/10.1029/2021JF006161

Received 15 MAR 2021
Accepted 14 JUL 2021

Author Contributions:

Conceptualization: Antoine Rabatel, Christian Vincent
Data curation: Diego Cusicanqui, Emmanuel Thibert
Formal analysis: Diego Cusicanqui, Antoine Rabatel, Christian Vincent, Xavier Bodin, Emmanuel Thibert
Funding acquisition: Antoine Rabatel, Xavier Bodin
Investigation: Diego Cusicanqui, Xavier Bodin, Emmanuel Thibert

Abstract Rock glaciers are creeping bodies of ice and rock that account for an important part of the mountain cryosphere. In this study, we investigated long-term changes of the Laurichard rock glacier (French Alps), to understand how this rock glacier is responding to climate change. Using feature-tracking and photogrammetric measurements between 1952 and 2019, we quantified changes in thickness, flow velocities and from which we derived the ice/rock flux of the rock glacier at a decadal time scale. This is the first time that emergence velocity and surface mass balance changes have been reconstructed for a rock glacier. Our results reveal a very small surface mass balance ranging from −0.1 m a^{-1} to +0.05 m a^{-1}, reflecting the role of debris in damping the melt rate of the underlying ice. Surprisingly, we found a more negative surface mass balance in the upper part than in the lower part of the rock glacier during the 1952–1971 cold period, likely due to a reduction in rock and snow mass accumulation. Our study shows that thickness changes are mainly driven by changes in surface mass balance except during the most recent period in the lower part of the rock glacier, which was also influenced by a compressive flow related to a protrusion that prevented the rock glacier from advancing. We conclude that the period 1994–2019 witnessed a marked acceleration in rock glacier flow, in agreement with the observations of other rock glaciers in the European Alps. This strong increase in surface speed is likely a consequence of changes in the basal conditions.

1. Introduction

Glacial and periglacial environments are highly sensitive to climate change (e.g., Dyurgerov & Meier, 2000; Trenberth et al., 2007). In mountains, perennial cryosphere features like glaciers and permafrost are highly impacted by climate forcing and have undergone rapid changes in recent decades (Haeberli et al., 1993; Hock et al., 2019; Oerlemans, 2005). In the European Alps, glacier retreat (e.g., Beniston et al., 2018; Davaze et al., 2020; Huss, 2012; Huss et al., 2017) and permafrost thawing (e.g., Harris et al., 2001; Haeberli et al., 2010; Marmy et al., 2016; Mollaret et al., 2019) have destabilized mountain slopes, thereby threatening human infrastructures and inhabitants (e.g., Deline et al., 2015; Duvillard et al., 2019; Huggel et al., 2015; Marcer et al., 2020, 2021; Schoeneich et al., 2015). In such mountainous environments, the interaction between different processes related to snow, ice, permafrost, and water availability, often intensified by the steepness of the terrain, may lead to cascading and chain reaction phenomena, that are occasionally transformed into catastrophic events, such as the Piz Cengalo landslide cascade in summer 2017 (Walter et al., 2020).

Measuring and interpreting surface kinematics of rock glaciers has been an important research field for several decades, the scales ranging from multiannual (e.g., Barsch, 1996; Bodin et al., 2009, 2018; Hartl et al., 2016; Kääb et al., 2021, 1997; Kellerer-Pirklbauer et al., 2018) to seasonal (e.g., Buchli et al., 2018; PERMOS, 2016) and short-term (daily) scales (e.g., Kenner et al., 2017; Wirz et al., 2016). Rock glacier kinematics are widely considered to be a key variable of the relationships between climate and mountain permafrost (Delaloye et al., 2018). The internal deformation of rock glaciers has been investigated less frequently, using borehole inclinometers (e.g., Arenson et al., 2002; Buchli et al., 2018; Kenner et al., 2017). These studies have shown that deformation has two main components: Internal plastic deformation of the ice-rich permafrost body and shearing concentrated in a horizon a few meters thick located at a depth of

Methodology: Diego Cusicanqui, Christian Vincent
Supervision: Antoine Rabatel, Christian Vincent, Xavier Bodin
Validation: Antoine Rabatel, Christian Vincent, Xavier Bodin, Emmanuel Thibert
Visualization: Diego Cusicanqui
Writing – original draft: Diego Cusicanqui, Antoine Rabatel, Xavier Bodin
Writing – review & editing: Diego Cusicanqui, Antoine Rabatel, Christian Vincent, Xavier Bodin, Emmanuel Thibert, Bernard Francou

between 15 and 30 m, where it has been documented to produce 60%–90% of the total deformation recorded at the surface (Cicoira et al., 2021; Springman et al., 2012).

Recent studies recorded an acceleration of the flow of many Alpine rock glaciers at an interannual scale in the last two to three decades, resulting in increasing surface displacement rates ranging from decimeters up to several meters per year (e.g., Delaloye et al., 2008; Eriksen et al., 2018; Hartl et al., 2016; Kellerer-Pirklbauer et al., 2018; Kenner et al., 2019). Several hypotheses have been proposed to explain this acceleration. One is the dependence of ice viscosity on temperature (Mellor & Testa, 1969). This hypothesis suggests that changes in rock glacier deformation would be influenced by variations in air temperature (e.g., Kääb et al., 2007; Delaloye et al., 2010; Wagner, 1992). Air temperature influences the internal temperature of the rock glacier and consequently the viscosity of the ice-debris mixture (Cicoira, Beutel, Faillettaz, Gärtner-Roer, & Vieli, 2019). However, a recent work concluded that the effect of heat conduction alone cannot explain an increase in viscosity that would have led to the observed changes in surface velocities (Cicoira, Beutel, Faillettaz, Gärtner-Roer, & Vieli, 2019).

To complete and go beyond the limited effect of temperature, several recent studies emphasize the influence of the water drainage system on the deformation rate of rock glaciers, especially within the shear horizon (Buchli et al., 2018; Cicoira, Beutel, Faillettaz, & Vieli, 2019; Jansen & Hergarten, 2006; Kenner et al., 2017; Wirz et al., 2016). The presence of water in rock glaciers has been suspected (Zenklusen Mutter & Philips, 2011) or observed in deep taliks (a layer of unfrozen material in the permafrost) in rock glaciers (Buchli et al., 2018). It has been suggested that when snow-melt water percolates into the shearing layer through taliks, it could cause a drastic increase in the deformation recorded at the surface in spring (Kenner et al., 2017). More recent works by Cicoira, Beutel, Faillettaz, and Vieli (2019) used a process-based model and successfully reproduced the seasonal variation in velocity. Overall, these results suggest that particularly in the shear horizon where shearing occurs, the effect of pore water pressure on rock glacier flow is greater than the effect of ice temperature on viscosity or shear resistance. In contrast to temperate Alpine glaciers where basal sliding is a major component of the observed surface displacements, no such basal sliding has been reported in rock glaciers to date. This may be partly explained by the roughness of the interface between the rock glacier and its bed, although other mechanical properties of rock glaciers may also play a role.

As mentioned above, changes in rock glacier dynamics are reflected in changes at the surface (Whalley & Azizi, 1994). However, volumetric changes (i.e., variations in thickness and in surface area) have received less attention. Some authors (e.g., Abermann et al., 2010; Bollmann et al., 2015) suggest that these volumetric changes are related to rock glacier dynamics (i.e., mass advection in the frontal part of the rock glacier). On the other hand, overall thinning of a rock glacier is frequently attributed to ice melt (Harris et al., 2001), although changes in effective debris production of rock wall weathering and the relative area of active versus inactive portion of the rock wall during cooler climates may also play a role (Refsnider & Brugger, 2007).

Despite all the above hypotheses, very few studies have been dedicated to rock glacier dynamics (e.g., Anderson et al., 2018; Cicoira et al., 2021; Frehner et al., 2015; Jansen & Hergarten, 2006; Olyphant, 1983). Many questions thus remain concerning the factors that drive changes in rock glacier dynamics at the time scale of a few decades. Analyses of surface displacement alone are not sufficient to understand the behavior of rock glaciers. In the present study, we therefore propose to rely on the continuity equation for ice flow in order to analyze and understand the changes in the rock glacier dynamics. This approach, detailed in Section 3.5 (Equation 4) and taken from Cuffey and Paterson (2010, Chapter 8) is applied on the 67-year data set of measurements made on the Laurichard rock glacier (French Alps). For that, we used photogrammetric measurements and feature tracking image correlation techniques to analyze changes in surface elevation, surface velocities, rock glacier thickness, and volume fluxes. In addition, we reconstructed the emergence velocities and surface mass balance to provide insights into the causes of the behavior of this rock glacier.

2. Study Area and Climatic Settings

The Laurichard rock glacier is located in the *Combe de Laurichard* catchment that belongs to the Ecrins National Park, Southern French Alps (45.01°N, 6.37°E, Figure 1). The peak of *Roc noir de Combeynot*, at whose foot the rock glacier is located, is characterized by a steep rock wall extending from 3,112 m a.s.l. at

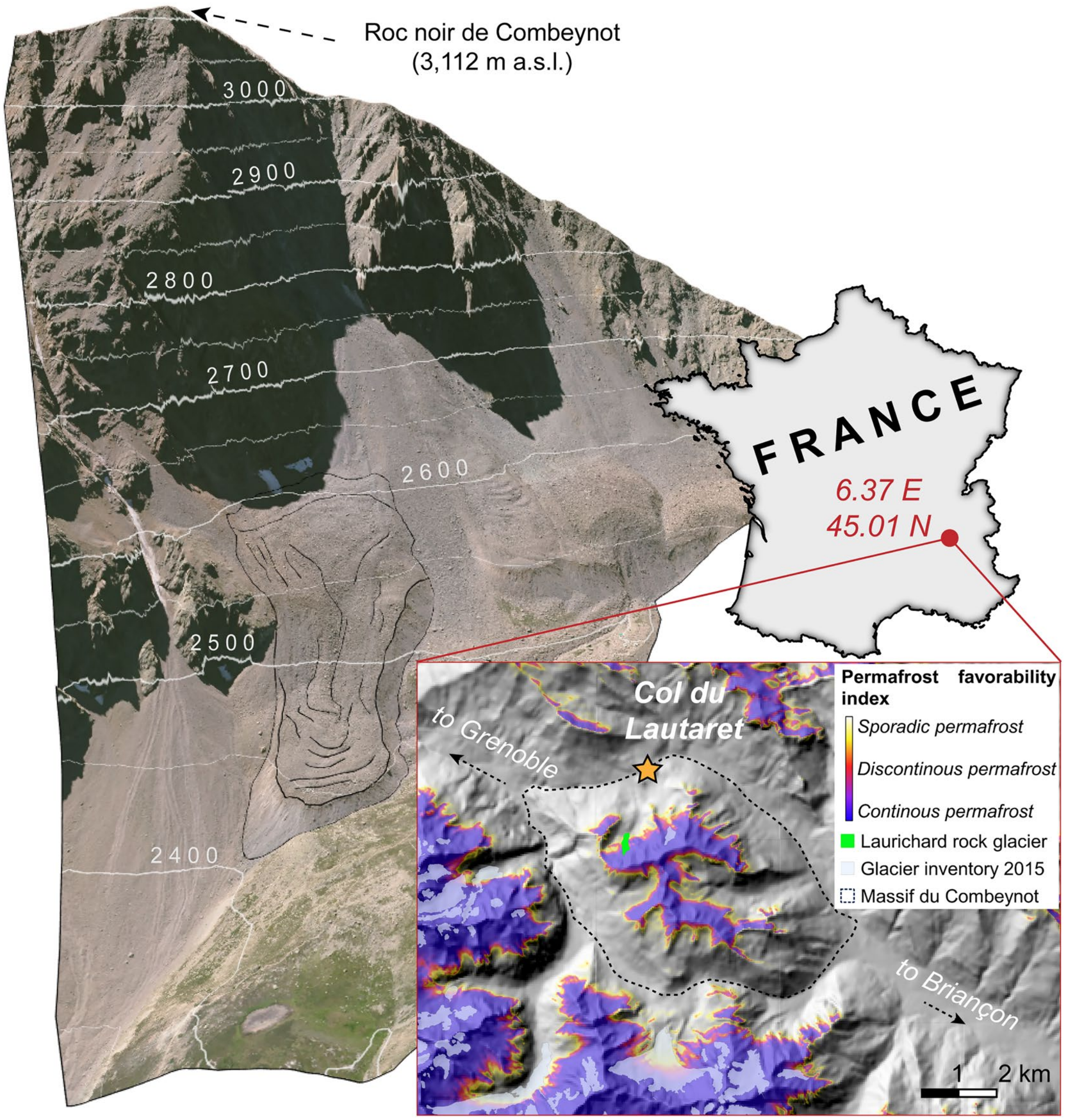

Figure 1. Perspective view of the Laurichard rock glacier in the Combeynot massif (image acquired in 2018). The inset (after Marcer et al., 2017) is a permafrost favorability index map distribution in the French Alps showing the extent of glaciers in 2015 (Paul et al., 2020).

the summit down to ∼2,600 m a.s.l. at the rooting zone of the rock glacier. The elevation and the predominant northern orientation of the site allow the presence of permafrost (inner map in Figure 1 adapted from Marcer et al., 2017).

The Laurichard rock glacier has a rather simple tongue-shaped morphology (500 m long and 100–200 m wide) typical of the rock glaciers in the region according to existing inventories (Marcer et al., 2017). It extends from 2,620 m a.s.l. at the rooting zone where the rock glacier is in contact with the rock wall and ends at 2,430 m a.s.l. at the terminus. The mean elevation of the rock glacier (2,556 m a.s.l.) is ∼100 m lower than the mean elevation of other North-facing active rock glaciers (2,655 m a.s.l.) inventoried in the French Alps (Marcer et al., 2017).

The main source of debris is the rock wall above the rock glacier that supplies relatively large boulders (decimetric to metric), mostly during the snow melting period (Coutard & Francou, 1989). In addition to the supply of debris, the rock wall topography, with several corridors (*couloirs*) that cross it, is also responsible for an important avalanche activity. This is evidenced in the field by typical deposits (Jomelli &

10.1029/2021JF006161

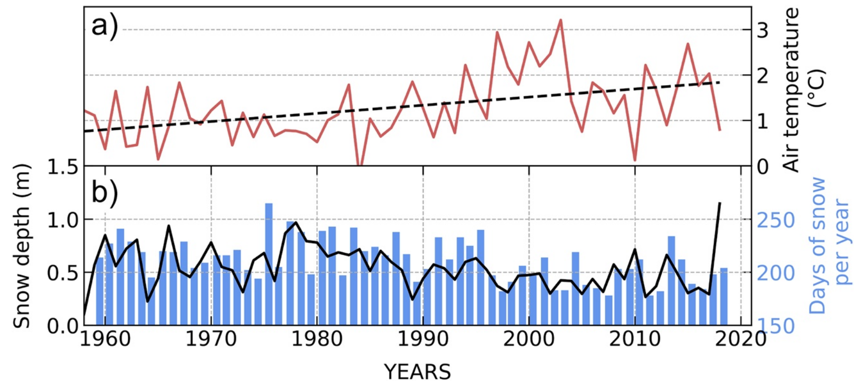

Figure 2. (a) Average annual air temperature (the black dotted line represents the linear trend), (b) annual snow depth (black line) and total number of days per year with snowfall (blue bars) retrieved from S2M weather data reanalyses for the period 1958–2018, corresponding to an elevation of 2,400 m a.s.l., a terrain with northern exposure and a 20° slope in the Ecrins range (Oisans massif in the S2M data set) that represent the characteristics of the Laurichard rock glacier site.

Francou, 2000), and the snow accumulated by avalanches often covers large parts of the rooting zone of the rock glacier down to about 2,550 m a.s.l.

The steepest surface slope of the rock glacier (∼45°) is found in the upper section of the frontal talus and the least slope (∼35–37°) in the middle section of the rock glacier, at an elevation ranging from 2,490 to 2,550 m a.s.l.

In situ topographical measurements on blocks distributed along rectilinear profiles started in the late 1970s in order to quantify the annual surface velocities of the rock glacier (Francou & Reynaud, 1992). This monitoring continues today (Thibert et al., 2018), and these in-situ data were used for validation purposes in our study. Several vertical electrical soundings (Francou & Reynaud, 1992) and electrical resistivity tomography (Bodin et al., 2009) enabled the estimation of the internal composition of the rock glacier as: (a) An ice-free 1 to 6-m thick upper layer composed of coarse blocks, except on the ridges where a finer matrix is also locally visible at the surface; (b) high resistivity values in the rooting zone suggesting the presence of an ice-rich layer, between 15 and 30 m thick, that corresponds to a core of massive ice also observed in 2003 in a *"rimaye"* (also known as the "bergschrund"). More detailed information can be found in Bodin et al. (2009) and Francou and Reynaud (1992). Low resistivity values measured in the tongue suggest the presence of a discontinuous ice layer and the presence of water. Finally, beneath this ice-rich layer is found (c) the interface with the bedrock.

To assess the climatology of the area, time series of temperature, and snow depth on the Laurichard site (elevation 2,400 m a.s.l., northern exposure, 20° slope) for the period 1958–2018 (Figure 2) were retrieved from the S2M data set that provides weather reanalyses (SAFRAN data from Durand, Giraud, et al., 2009; Durand, Laternser, et al., 2009; Vernay et al., 2020). Marked year-to-year variability characterized both air temperature (annual average for period 1958–2018: 1.3 ± 0.76°C at 2,400 m a.s.l.) and snowfall (791 ± 169 mm yr^{-1}). Snowfall showed no particular trend or change over the 60-year period, although the mean number of days of snow cover during winter decreased from 221 in the period 1958–1990 to 200 in the period 1990–2018. The reverse applies to air temperature, which was significantly higher after the early 1990s than before (average for the 1958–1990 period, 1.0 vs. 1.7°C for the period 1991–2018), that is, a change of +0.23°C per decade (Figure 2).

3. Data and Method

The method used in this study was based on digital surface models (DSMs) and orthorectified images, both generated from historical aerial images using photogrammetry. From this multiannual data set, we derived: (a) surface displacement maps through the correlation of pairs of orthorectified images; (b) maps of changes in surface elevation quantified from differences in DSM (DoD); and (c) we quantified changes in

Table 1
Details of Aerial Imagery Used as Input Data and Reference Data (the Reference Data Set is in **Bold***)*

#	Acquisition date	Scale	N° of photos	N° of GCPs	Type	Format	% Overlap across/along the track
1	August 1, 1952	~1/31,000	4	9	B&W	Film	60/50
2	August 22, 1960	~1/25,800	3	11	B&W	Film	–/80
3	August 16, 1971	~1/26,200	3	12	B&W	Film	–/80
4	September 6, 1986	~1/31,000	3	10	B&W	Film	–/80
5	August 3, 1994	~1/22,000	6	13	IR	Film	60/80
6	July 5, 2003	~1/19,100	3	14	RGB	Film	–/80
7	**August 17, 2012**	**50 cm**	–	–	**LiDAR**	–	–
8	August 10, 2013	~1/30,000	6	13	RGB	Digital	40/80
9	October 5, 2017	~1/500	158	21 (12[a])	RGB	Digital	60/80
10	July 23, 2019	~1/250	322	13 (7[a])	RGB	Digital	60/80

[a]Refers to ground control points deployed inside the rock glacier.

thickness and fluxes by estimating bedrock geometry using ground-penetrating radar (GPR) measurements and surface mass balances.

3.1. Aerial Imagery and UAV Acquisitions

We obtained historical aerial photographs dated ~1950–2013 from the aero-photography library run by the "French National Institute for Geographic information" (French acronym, IGN: https://remonterletemps.ign.fr/) (Plu & Ducher, 1988; Rodríguez et al., 2008). The 10 campaigns listed in Table 1 were used in this study: seven aerial photograph surveys, one aerial LiDAR survey, and two uncrewed aerial vehicle (UAV) surveys. The aerial surveys were selected based on the following criteria: (a) a minimum of three photographs available per campaign covering the sector; (b) the scale of the images had to be better than 1:50,000; (c) limited snow cover, given the aspect and high altitude of the rock glacier (snow patches may persist for several years); and (d) a long enough time interval (~8–10 years), which is needed to obtain a significant signal-to-noise ratio to quantify the surface displacement (considering the typical 1 m of annual movements of this rock glacier; Thibert et al., 2018). For the current study, we processed 31 aerial images (from seven sets covering 60 years) of varying quality, scale, and overlap (details are listed in Table 1).

Because no aerial photographs of the Laurichard rock glacier are available after 2013, for 2017 and 2019, we used images acquired by a UAV. For 2017, we used a UAV survey (DJI Phantom 4 quadcopter) made on October 5, 2017 for a previous study (Goetz et al., 2019). For 2019, we used a UAV image acquired on July 23, 2019 using a DJI Phantom 4 real-time kinematic (RTK). For these two acquisitions, independent ground control points (GCPs) were measured along the sides and on the surface of the rock glacier (see Table 1 for details) using a Trimble SPS351 differential global positioning system/Beacon (DGPS) receiver using a local permanent GPS station located at the Joseph Fourier Alpine station (SAJF, https://www.jardinalpindulautaret.fr/) close to the *Col du Lautaret* at 2,080 m a.s.l. and less than 2 km from the study site. Additionally, two permanent GNSS stations belonging to the RGP network (http://rgp.ign.fr/) were used in the post-processing stage. Vertical and horizontal precision better than ±0.05 m was found for all GCPs.

For the processing of the IGN aerial photo, an aerial laser scanning image acquired on August 16 and 17, 2012 was used as reference data for altimetry and planimetry. The accuracy of the point cloud was estimated at ±0.1 m in planimetry and ±0.25 m in altimetry, and a density of 7 points/m^2 was available to build the final DSM with a spatial resolution of 0.5 m (SINTEGRA, 2012). This DSM was also used to extract additional GCPs for photogrammetric processing of the aerial photographs. To select these GCPs, all the aerial photographs used were first examined visually to select a stable area common to all images. We then selected features according to a single requirement: all GCPs must be visible on the images of each survey. Once the features were selected, their XYZ coordinates were extracted from the LiDAR reference DSM (Table 1).

3.2. Rock Glacier Thickness and Bedrock Estimation

GPR is a geophysical technique commonly used to document the internal structure and thickness distribution of rock glaciers (e.g., Gruber & Ludwig, 1996; Jol & Bristow, 2003; Monnier et al., 2008, 2009; Reynolds, 2011). GPR data for the Laurichard rock glacier were acquired at the end of June 2019, when remnants of snow on the terrain facilitated the survey. The specifications for this acquisition are detailed in Guillemot et al. (2021). Briefly, processing of the GPR data included normal moveout corrections (NMO) to compensate for the source-receiver offset of 6 m on 25 MHz RTA antennas, migration, and time-to-depth conversions. For the latter processes, a mean 12 cm ns^{-1} velocity was used, estimated from a single common Middle Point 100 MHz velocity analysis. The data were then analyzed in different frequency bands, which helped to select the main basal reflector. Based on velocity and selection, uncertainties, and the wavelength, Guillemot et al. (2021) estimated the reflector accuracy to be maximum ± 3 m.

Figure S1 illustrates the 260-m long longitudinal GPR profile along the central flow line between 2,580 and 2,460 m a.s.l. This profile allowed us to estimate the geometry of the interface between the rock glacier and its bed, which we call "bedrock," even though it may be either bedrock or debris. These data enabled the quantification of the thickness along the central flow line. Based on these thickness values and on the contour lines on the stable terrain on each side of the tongue of the rock glacier, the bedrock was manually interpolated over the entire rock glacier. For that purpose, we first masked the rock glacier area, and then drew the contour lines starting from the surrounding stable terrain and the elevation of the bedrock interface at the level of the central flow line quantified using the GPR data (Figure S1).

This way of establishing the Digital Terrain Model (DTM) of the bedrock, although partly subjective, was allowed by: (a) the high quality of the topographical data available for the stable area (LiDAR DSM); (b) the narrow and elongated shape of the rock glacier with well-defined boundaries; and (c) the availability of the longitudinal GPR profile, which covered 60% of the total length of the rock glacier. The results obtained by Guillemot et al. (2021) on a transverse profile of the tongue of the Laurichard rock glacier locally suggest good agreement between the DTM of the bedrock (which these authors also used) and the inverted thickness retrieved from the modal analysis of the independent seismic data set.

3.3. Digital Elevation Models and Orthoimagery

All the aerial photographs used for the DSMs and orthoimagery production were processed using structure-from-motion (SfM) techniques (Smith et al., 2015) with Agisoft Metashape software (version 1.6). This popular software provides workflow for DSM and orthomosaic generation and has been shown to perform well for DSM production on high-alpine rock glaciers (e.g., Mertes et al., 2017; Mölg & Bolch, 2017; Piermattei et al., 2015).

However, in the present study, one challenge was processing historical aerial photographs that are usually of low quality not only in terms of resolution but also of geometry (i.e., radial distortion, rectangular frames in the case of the oldest photographs dating from ∼1950). Additionally, the texture and contrast of the images, which are often a limitation considerably influence the accuracy of the final DSMs and orthoimages (Micheletti et al., 2015).

The DSMs and orthoimages for each survey were generated at the maximum resolution allowed by the software (high resolution point cloud) and *"Moderate depth filtering"* (except for surveys conducted in 1952, 1960, and 1971 for which *"Mild depth filtering"* was used). Because the resulting resolution of the products of the different surveys was not the same, we resampled the resolution to 1 m for all the DSMs and to 0.5 m for all the orthoimages except those acquired in 1952 and 1960, which we resampled at 1.5 m.

To improve the consistency of the products, we performed a co-registration using the method of Nuth and Kääb (2011) by assuming that the terrain surrounding the rock glacier is stable. The stable area used for co-registration, although limited to 0.9 km^2, was selected on the basis of a detailed visual check of the photographs and geomorphological evidence gathered during field campaigns to be sure no important morphological changes had occurred over the entire study period (details of this step are provided in Table S1).

To assess the quality of the resulting DSMs, each was compared with our reference 2012 DSM generated by LiDAR. First, the stable terrain area in front of the rock glacier was used to quantify the uncertainties

(Figure S2a). As expected, the mean differences between each DSM and the reference data showed that the DSMs established based on the oldest data (DSMs from 1952 until 1986) had the highest uncertainties, ranging from 0.5 to 1.1 m in elevation. An uncertainty of less than 0.25 m was found for the other DSMs from 1994 to 2019 (for details, see Table S2).

We also used four profiles located in the stable area (Figure S2c) where uncertainties for the DSMs from 1952 to 1986 were between 0.4 and 1.2 m and those for the other DSMs were less than 0.3 m. The biggest differences were found at the beginning of "Profile V1", where some artifacts were identified, likely due to the poor contrast and low resolution of the images, and in "Profile V3", where the slope increases (Figure S2c). The biggest differences (+6 and −4 m) were found for the year 1952 and correspond to the presence of snow patches close to the border of the rock glacier and to artifacts due to poor contrast and quality.

As shown in Figure S2b, the co-registration step allowed us to reduce the uncertainties of DSMs by ∼15% for the years 1952, 1960, 1971, and 1986 (equivalent to 0.10 m, i.e., reducing the difference from ±1.16 m to ±1.06 m for 1952), by ∼5–10% for DSMs generated using the data collected between 1994 and 2013 (equivalent to 0.05 m), and by ∼30% for the UAV acquired in 2017 and 2019, that is, equivalent to ∼0.12 m, after co-registration.

A final validation was conducted using independent data from the total station and d-GNSS measurements of block coordinates, and the final co-registered DSMs were made to evaluate the quality of the data inside the rock glacier (Thibert et al., 2018). These values are reported in Figure S6 and show that the accuracy of the DSMs is within a ±1 m interval (the oldest DSMs had the highest deviations) with an average median value of 0.2 m, consistent with the accuracy limits previously established for the stable area. Part of this deviation from d-GNSS positions is probably due to the block geometry that may not be accurately reproduced by the photogrammetric DSMs, because of their size (decimetric to metric) and shape (steep with sharp angular facets). However, overall, this comparison gave us sufficient confidence to calculate the differences in the DSMs.

3.4. Quantification of Horizontal Surface Displacements

We computed spatial fields of 2D surface displacements using feature-tracking image correlation techniques. The data were processed using the IMCORR algorithm in SAGA-GIS software (e.g., Conrad et al., 2015; Scambos et al., 1992). Several parameters of the algorithm were tested, and finally, we used the following: search chip size = 128 pixels; pattern chip size = 64 pixels; and grid interval = 5 pixels. This configuration allows the feature-tracking step to produce the most coherent results in terms of spatial distribution and displacement values. However, for the oldest period, due to the coarser resolution of the data, we adapted the size of the search chip to 64 pixels and that of the pattern chip to 32 pixels, while keeping the same grid interval. This involved a 30% reduction in the density of points.

Subsequently, we applied a semiautomatic filtering procedure with the following requirements: (a) direction of the displacement must be consistent between neighboring vectors (difference < 30°); (b) correlation points were eliminated in areas where snow patches and shadows are present on at least one of the two DSMs (these areas represent up to about 15% of the rock glacier area, mainly in the upper part); and (c) outlier displacement values (defined as 2D displacements >20 m per period) were directly removed. The remaining outliers were removed manually after a visual inspection and checking consistency with their neighbors. Finally, between 55% and 70% of the original points were conserved and used for the interpolation of the surface flow velocities. The interpolation was performed using the inverse distance weighted method on a 3-m resolution grid (Figure 5).

The uncertainties of the image correlation step were estimated based on the stable terrain (Figure S2) surrounding the rock glacier, which represented an area of 0.1 km^2 (Table S3).

To validate the surface displacements, we used in-situ topographical measurements of individual marked blocks that started in the early 1980s (Francou & Reynaud, 1992). These blocks are located along a central longitudinal profile and two transverse profiles in the upper and lower reaches (Bodin et al., 2009; Thibert et al., 2018). As shown in Figure S3, the overall agreement between *in-situ* measurements and correlation results is very good (mean RMSE of 0.01 m a^{-1} and r^2 varying between 0.94 and 0.98 for the five different

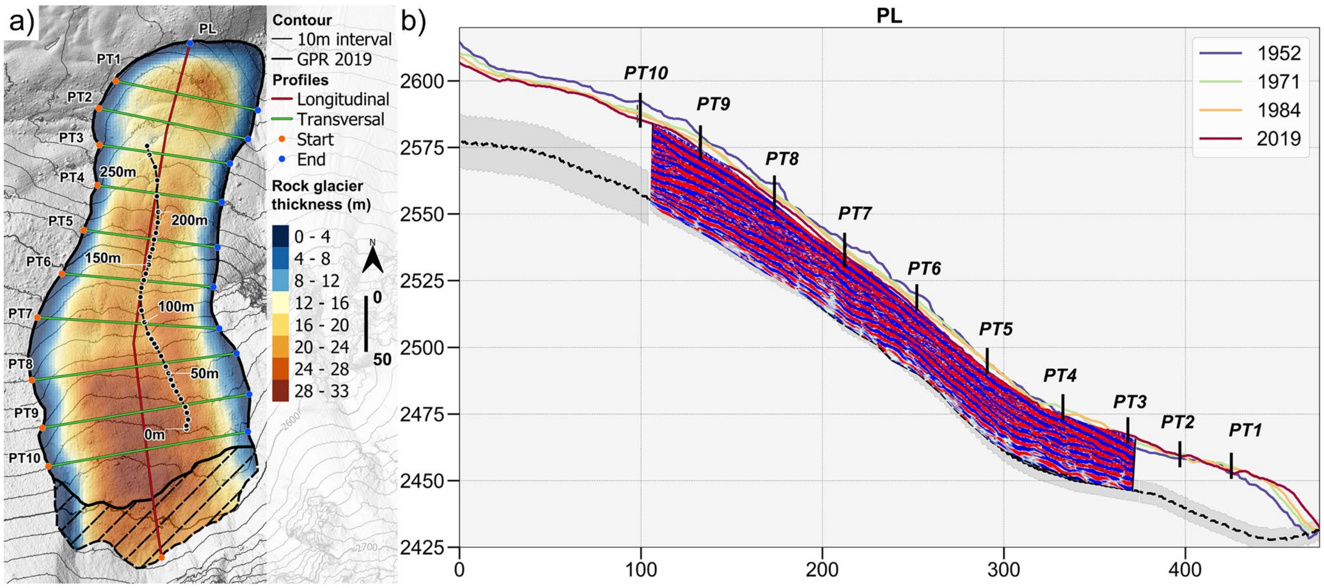

Figure 3. (a) Absolute rock glacier thickness in meters, after the interpolation of ground penetrating radar (GPR) profile and extrapolation from contour lines outside the rock glacier. The dashed area on the upper part of the rooting zone in the left panel corresponds to an excluded sector where images could generally not be processed (due to shadows and snow cover). (b) Longitudinal profile on the central line showing the position of the bedrock using GPR profile (25 MHz data adapted from Guillemot et al., 2021), the location of transversal profiles, and surface elevation along the rock glacier in 1952, 1971, 1994, and 2019. The complete GPR profile used for bedrock estimation is shown in Figure S1.

periods). The main differences are due to the velocities quantified close to the rock glacier edges (low velocity areas), where differences reached 0.30 m a^{-1} in the worst cases (Figure S3). Note that some of the difference may result from the time interval between the aerial and field surveys, which was 23 days on average (but up to 109 days in 2019); considering that the rock glacier flows close to 1 m a^{-1}, this gives a difference of 0.06 m a^{-1} (up to 0.4 m a^{-1} for 2019).

3.5. Fluxes and Surface Mass Balance Quantification

We quantified the surface mass balance in several sectors of the rock glacier using volumetric fluxes through cross sections and changes in surface thickness. For this purpose, we delineated 10 transverse profiles at 30–40 m intervals numbered from the terminus (PT1) to the upper reaches (PT10) (Figure 3). The flux was calculated for each of these cross sections down to the bedrock. Note that the fluxes are expressed in m^3 a^{-1} (volume flux) and that no assumptions were made concerning the density of the material to provide a mass flux as discussed above.

The flux of volume Q (m^3 a^{-1}) through each cross section was calculated using the cross-sectional area S_c (m^2) and depth-averaged horizontal velocity U_d (m a^{-1}).

$$Q = U_d S_c, \tag{1}$$

U_d was derived from the mean surface velocity, U_s. According to Nye (1965), the ratio F between the depth-averaged horizontal velocity and the mean surface velocity varies from 0.8 to 1 (no sliding and maximum sliding) for a glacier. Here, we assume that the rheology of this rock glacier is similar (no sliding) and consider that $F = 0.85$, such that $U_d = 0.85 \times U_s$. This value of F was also used in previous studies that used data on vertical deformation collected in boreholes (Arenson et al., 2002; Arenson & Springman, 2005; Cicoira et al., 2021; Springman et al., 2012). Equation 1 can be written as:

$$Q = U_s \; F \; L \; H_m, \tag{2}$$

where H_m is the mean depth of the cross section and L is the width of the cross section. Assuming that the random errors on U_s, F, and H_m are not correlated, the uncertainty related to the flux Q can be expressed as:

$$\sigma_Q^2 = \sigma_{Us}^2\ F^2\ L^2\ H_m^2 + \sigma_F^2\ U_s^2\ L^2\ H_m^2 + \sigma_{Hm}^2\ U_s^2\ F^2\ L^2, \tag{3}$$

We assume that the uncertainty on F is roughly 10% (Anderson & Anderson, 2016; Müller et al., 2016; Nye, 1965). The uncertainties on H_m and U_s are assumed to be 3 m and 0.08 m a^{-1}, respectively. The average width of the cross sections is 150 m, leading to an uncertainty of 476 m^3 a^{-1}, which corresponds to about 28% of the calculated flux Q.

Following the continuity equation (Cuffey & Paterson, 2010, p. 286 and p. 333), the change in surface elevation can be expressed as a function of the surface mass balance (b_s) and the difference in ice/rock fluxes between two sections:

$$\partial h/\partial t = b_s - \partial q/\partial x, \tag{4}$$

where q is the flux of volume per unit width across-flow, that is, $q = Q/L$, b_s the surface mass balance expressed in meters of a creeping mixture of rock and ice (m a^{-1}), $\partial h/\partial t$ is the average rate of change in thickness obtained between the cross sections.

The term $\partial q/\partial x$ represents the down-glacier gradient in ice discharge per unit width across-flow between two sections. $\partial Q/\partial x/A$, is the emergence velocity, and A is the surface area between the two cross sections.

In glaciology, emergence velocity is a standard way to link surface mass balance to changes in thickness. Emergence velocity represents the upward or downward flow of the ice relative to the glacier surface. Under steady-state conditions, this flow exactly compensates the surface mass balance (Cuffey & Paterson, 2010, p. 286). Finally, the uncertainties related to the surface mass balance can be calculated using Equation 5:

$$\sigma_{bs}^2 = \sigma_{\Delta h}^2 + \sigma_{\Delta Q}^2, \tag{5}$$

Use of the term "surface mass balance" can be questioned for several reasons. Surface mass balance (which represents accumulation and ablation processes) is a standard in glaciology, but some major differences have to be taken into account for rock glaciers. First, the accumulation processes differ given that both ice and rocks accumulate in the upper reaches of the rock glacier. Ice originates from the compaction of snow (when overlaid by rock falls and/or the snowfall in successive winters, Giardino et al., 1987) but may also originate from the refreezing of surface melt water at depth (i.e., internal accumulation) if the internal temperatures are negative. In addition, large quantities of debris originating from the rock falls accumulate on the surface (Haeberli et al., 1998). On the other hand, ablation processes not only occur at the surface only but also in the sub-surface under the layer of debris (Anderson et al., 2018; Evatt et al., 2015; Harris et al., 2001).

Using the term "surface mass balance" raises another question regarding density values that need to be taken into consideration to estimate changes in mass. Due to the complex and peculiar internal structure of a rock glacier (mixture of ice and debris, different proportions of more or less uniformly distributed massive ice depending on where the ice is located within the rock glacier) the density of the material that comprises the rock glacier varies considerably in space and is in fact unknown. A few studies addressed this issue using borehole data (e.g., Haeberli, 1985; Haeberli et al., 1998, 2006) and showed that the density of the mixture of ice and debris typically found in a rock glacier is close to that of nonfrozen soils (1,500–1,800 kg m^{-3}).

In the present study, we chose not to account for density structure or how it may change because no information is available on ice content and ice distribution of Laurichard rock glacier and consequently quantified changes in surface volume rather than changes in mass. Thus, the term "surface mass balance" normally used for glaciers is not perfectly appropriate in the present case, but, as there is no adequate term for "rock glacier mass balance" (Cogley et al., 2011, p. 95); we therefore decided to use the same term for rock glaciers. It should also be noted that we did not convert the volume into water equivalent balance and that the unit of measure is therefore meters per year.

4. Results

4.1. Thickness Distribution Map

Figure 3 shows the distribution of estimated rock glacier thickness. It is worth recalling that from the surface down to the interface with the bedrock (or the debris that forms the base of the rock glacier, as defined in Section 3.2), starting from the surface, the internal structure of the rock glacier is likely composed of a shallow layer of blocks (generally called the "active layer" in the definition of permafrost) that contains no ice; followed by an ice-rich layer containing varying amounts of ice (Bodin et al., 2009). As shown in Figure S5, most of the rock glacier is concave at the interface with the bedrock (PT4–PT10). In the lowermost profiles (PT1–PT3), the shape of the bedrock morphology changes due to a change in the surrounding topography, that is, the tongue of the rock glacier flattens out as the slope decreases (see the longitudinal profile in Figure 3).

The average thickness of Laurichard rock glacier is 20 ± 3 m, in good agreement with previous estimates made using electrical resistivity (Bodin et al., 2009) and with modal analysis of seismic data (Guillemot et al., 2021). Some general features in Figure 3 can be highlighted. First, the upper area is noticeably thicker, reaching 30 ± 4 m between PT10 and PT8. The same pattern is also visible in a small portion of the rock glacier between PT4 and PT5 in the center and close to the terminus below PT1, the average thickness of both sections is 24 ± 4 m. Finally, the total volume of the rock glacier is estimated at 1,361,377 ± 280,000 m^3.

4.2. Changes in Surface Area and Elevation

Laurichard rock glacier has a well-defined shape with clear boundaries that help identify changes in geometry. The general shape of the rock glacier did not undergo any drastic changes between 1952 and 2019 except in its frontal sector, which advanced 13 m horizontally on average over the period (corresponding to 0.21 m a^{-1}) representing a 5% increase in the total surface area (the purple and red lines in the right panel in Figure 3). The increase in surface area was not even over the study period. Almost no changes were observed in the periods 1952–1960 and 1986–1994. Figure 4 illustrates the DSMs that differentiate each sub-period (Figures 4a–4h), and for the entire study period 1952–2019 (Figure 4i). Changes in elevation in the upper part of the rooting zone were not used for analysis due to the higher uncertainties on this part of the rock glacier caused by shadow and/or persistent snow cover in some years. The general pattern over the whole study period (1952–2019) (Figure 4i) was a decrease in the thickness (a lowering of the surface) of the whole body of the rock glacier, representing a total loss of 45,000 ± 550 m^3. Contrasted spatial patterns are also indicated: (a) lowering of the surface in the upper reaches of the rock glacier in red; (b) a thickening and an increase in surface elevation in the lower reaches in blue; with (c) in between, a mixed pattern, with thinning on the right and thickening on the left.

Considering the subperiods, there was a continual decrease in the overall rock glacier volume from 1952 to 1986 (Figure 4j) followed by an increase in volume from 1986 to 2003, and a further decrease after 2003. Note that, concomitantly with the increase in surface area, the surface elevation of the frontal sector (Figures 4a–4i, below PT1) increased by 10–15 m between 1986 and 2003.

4.3. Changes in Surface Velocities

Figure 5 illustrates the changes in surface velocity over each sub-period. The spatial pattern of velocity remained stable in the first four subperiods up to 1994 (Figure 5, upper panels). Over the 1952–1994 period, the average surface velocity calculated for the entire study area was 0.5 ± 0.09 m a^{-1}, with small patches where it reached 1.2 ± 0.09 m a^{-1} close to 2,500 m a.s.l. in the central part of the rock glacier tongue where the slope is the steepest (35°). During the following sub-period, 1994–2003, a major acceleration occurred throughout the landform, with 70% of the rock glacier surface presenting values higher than 0.5 ± 0.09 m a^{-1}, even the upper reaches of the rock glacier. The highest surface velocities, with displacement rates reaching between 1.5 and 2 ± 0.08 m a^{-1} on the central flow line, were recorded in the period 2013–2017. Finally, over the whole period, the average surface flow velocity doubled from 0.5 to 1 ± 0.09 m a^{-1}. The velocities obtained on each transverse profile for each period are shown in Figure 6b.

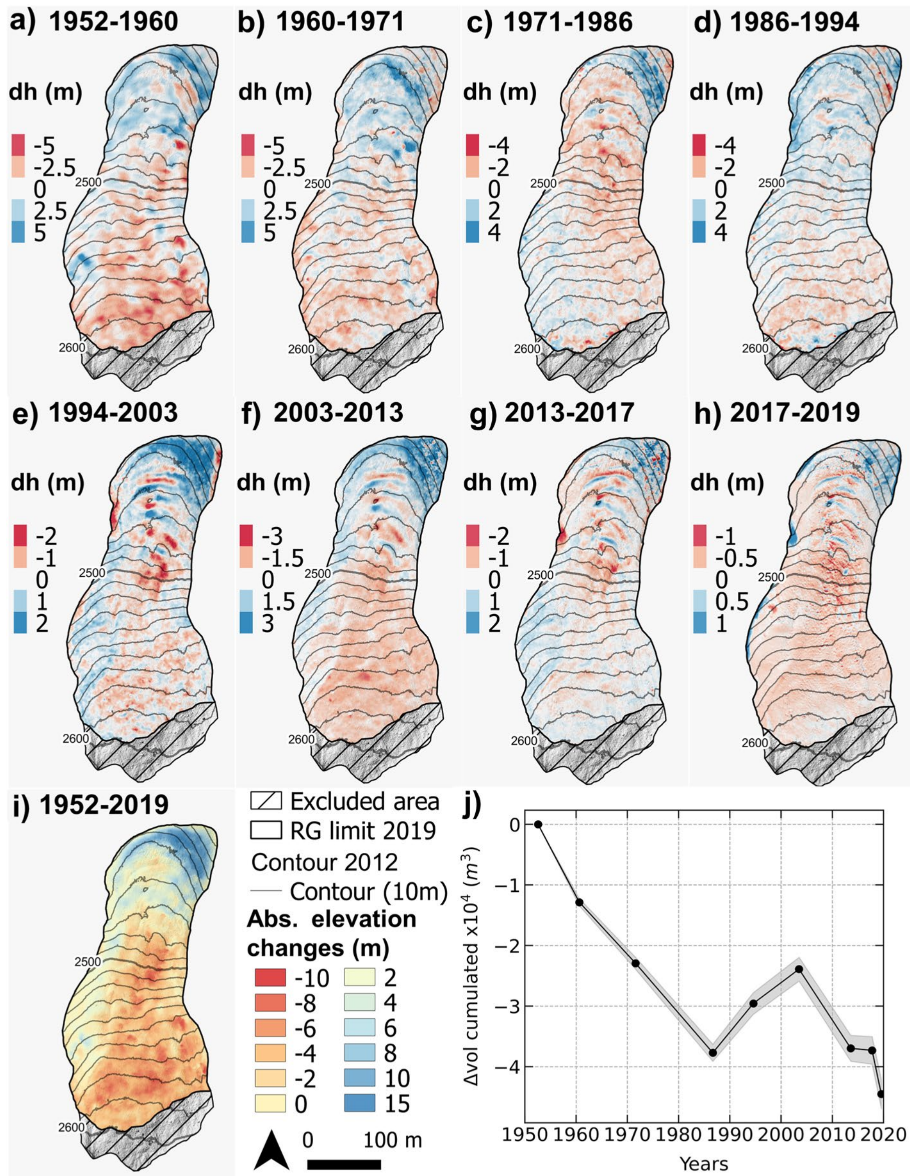

Figure 4. Changes in the surface elevation and in the volume of the Laurichard rock glacier during eight periods between 1952 and 2019, derived from differences in digital surface models. Each map (a–h) shows a specific sub-period while map i shows the entire study period. The color scale besides Panel i corresponds only to the longest period (1952–2019). Panel j shows the change in volume cumulated for the entire 1952-2019 study period.

It is noteworthy that, on the one hand, the above mentioned surface flow velocities are rather low (less than 1 m a^{-1} over most of the landform) and that, on the other hand, when considering the average thickness and slope of the rock glacier and applying the Glen's (1955) flow law for polycrystalline ice, the computed velocities are of the same order of magnitude as the observed ones. This would suggest that the Laurichard rock glacier behaves as if its internal creeping structure was mainly composed of ice. This would deserve to be confirmed by geophysical measurements and drilling data.

4.4. Fluxes Calculated for Each Cross Section

Considering the area of the cross sections (Figures 3 and S5) in each transverse profile (from PT1 to PT10) combined with surface velocities (Figure 5), we calculated the volume fluxes according to Equation 1. These fluxes are reported in Figure 6c. As mentioned in Section 3.5, the ratio F between the mean cross section

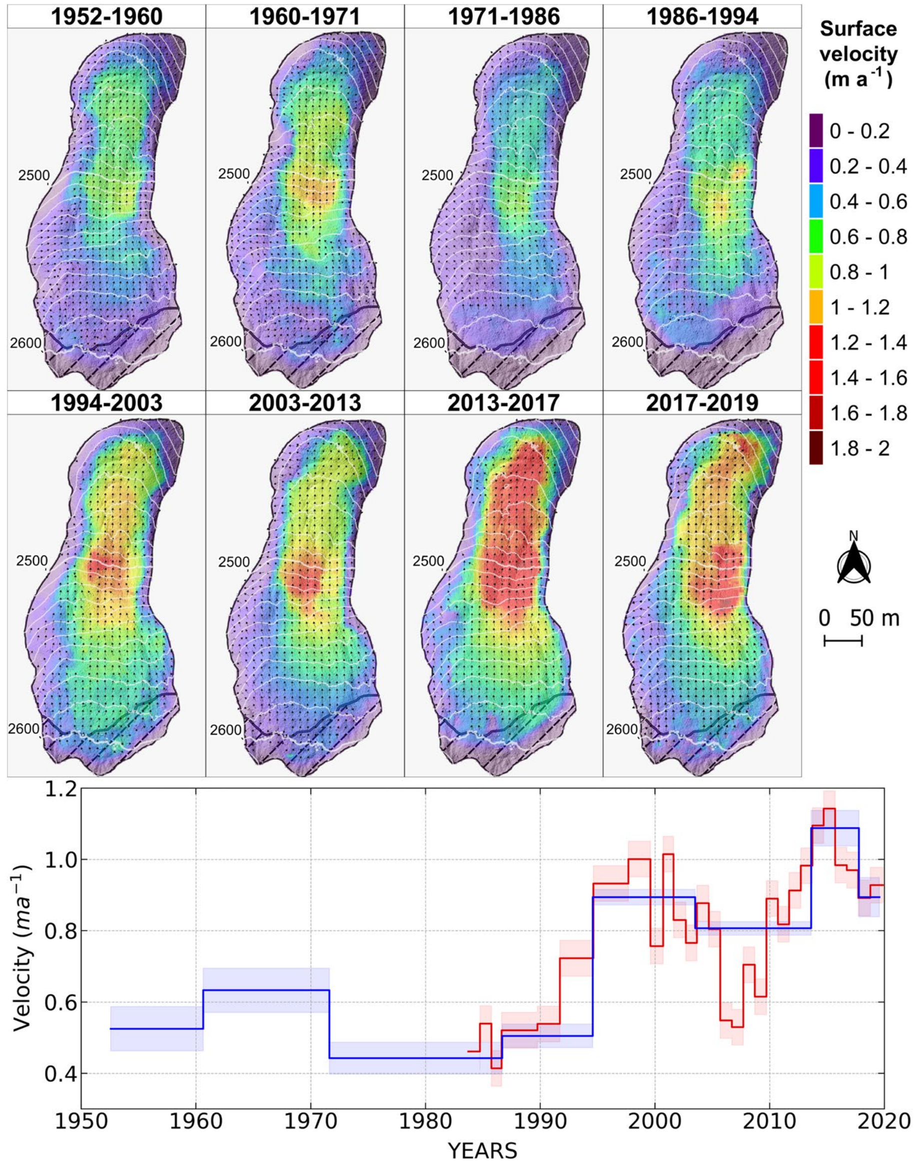

Figure 5. Upper panel, horizontal surface velocities of the Laurichard rock glacier between 1952 and 2019 in the eight different periods. Lower panel, the blue line shows mean horizontal velocity over the entire rock glacier and the red line shows the mean of the blocks. Block data were extracted from Thibert et al. (2018).

velocity and the mean surface velocity is assumed to be 0.85. The uncertainties related to F are discussed later. Some general features can be highlighted in Figure 6. First, the thickness decreased in the upper part of the rock glacier over the whole period (1952–2019) (Figure 6a), in contrast to the rock glacier tongue that almost continuously increased in thickness. Second, except for the marked acceleration after 1994, the fluctuations in surface velocities were similar throughout the rock glacier in the different periods (Figure 6b), although the increase in the surface velocities over the whole period was slightly more pronounced in the lower part. The fluxes were thus subject to the following variations over time (Figure 6c): an increase between 1952 and 1971, a decrease between 1971 and 1994, another increase between 1994 and 2017, and finally a decrease in the last two years of the observation period.

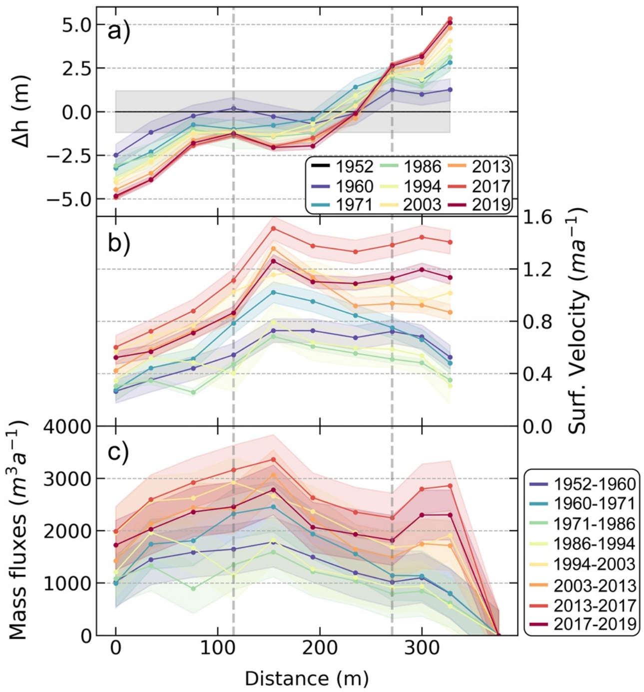

Figure 6. (a) Variations in thickness (Δh) computed using the 1952 surface DSM as a reference for each period; (b) Surface velocities extracted from the center flow line of the rock glacier; and (c) Fluxes for each period shown in (b). The *X*-axis corresponds to the distance in meters from profile #10 (PT10) down to the terminus; each colored dot corresponds to the location of a transverse profile along the *X*-axis (Figure S4), except for the last point of the flux curves, which is set outside. The vertical dashed gray lines correspond to the location of PT7 and PT3 (from left to right, which correspond to the sub-sections defined later and shown in Figure 7). Note that, in all panels, the semi-transparent colored areas behind each curve correspond to the uncertainty estimated after uncertainty propagation analysis (Tables S2 and S3 and Equation 3, respectively).

4.5. Reconstruction of Emergence Velocities and Surface Mass Balance

The calculated fluxes were used to reconstruct the surface mass balance between cross sections according to Equation 4. Given that the changes in elevation, surface velocity, and fluxes in the two consecutive periods were mostly close to or in the range of the uncertainties (Figure 6), a difficulty arose when we wanted to reconstruct the surface mass balance. To identify signals that are larger than uncertainties, in the following analysis we considered three regions and homogeneous periods of time for which changes in elevation, surface velocities, and fluxes were very similar as described below:

1. The upper region of the rock glacier, located between cross sections PT10 and PT7. In this region, the thickness decreased continuously over the whole period. The fluctuations in velocity were very similar, with a marked acceleration after 1994.
2. The intermediate region, located between PT7 and PT3. In this region slight changes in elevation occurred that were very similar throughout the period. Like in the upper region, the fluctuations in velocity also remained very similar from one period to another.
3. The lower region located between PT3 and the terminus. Here, there was a notable increase in thickness. Like in the two previous regions, fluctuations in velocity were very similar, with a marked acceleration after 1994.

Overall, the changes that occurred in each of the regions during each of the selected periods, 1952–1971, 1971–1994, and 1994–2019 were thus similar. However, thickening and acceleration over the last period were much more pronounced close to the terminus. This point somewhat contradicts our assumption of similar changes in all three regions and this point is discussed later. Finally, this differentiation between the thickening and acceleration allowed us to reconstruct emergence velocities and changes in the surface mass balance that exceed the uncertainties.

Figure 7 provides an overall picture of reconstructed emergence velocities and surface mass balance. First, the upper region (from PT10 to PT7) shows negative reconstructed emergence value (*or* submergence) velocities up to -3 ± 2 cm a^{-1}. The intermediate and lower sectors show increasingly positive values toward the rock glacier terminus that reached 2 ± 2–13 ± 2 cm a^{-1} in the lower sector, in agreement with the emergence of the ice flow lines. These values are also consistent with downward flow in the upper region and upward flow in the lower region often found in Alpine glaciers (Cuffey & Paterson, 2010, p. 233). In addition, the very similar emergence velocities obtained over the three observation periods mean we have confidence in our results. Note that the marked increase in the emergence velocity in the lower sector during the most recent period likely results from the compressive flow related to the terminus, when it encountered a protrusion that prevented the rock glacier terminus from advancing.

On the other hand, the reconstructed surface mass balance (Figure 7c) ranged from -0.1 m a^{-1} to $+0.05$ m a^{-1}, which is very low compared to mass balances reported for Alpine glaciers at similar altitudes (Vincent et al., 2017). It should be noted that the surface mass balance computed on Laurichard rock glacier is expressed in m a^{-1} and not in m w.e. a^{-1} (meter water equivalent per year) as used in glaciology, because it concerns changes in the overall volume of ice and rocks.

Finally, the reconstructed surface mass balance revealed a standard pattern in the second and third periods with a surface mass balance close to zero in the upper region and more negative values at lower elevations. In the first period (1952–1971), the pattern was a surprising reversed surface mass balance gradient, with negative values (-6 ± 4 cm a^{-1}) in the upper region and positive ones ($+4 \pm 4$ cm a^{-1}) in the lower part.

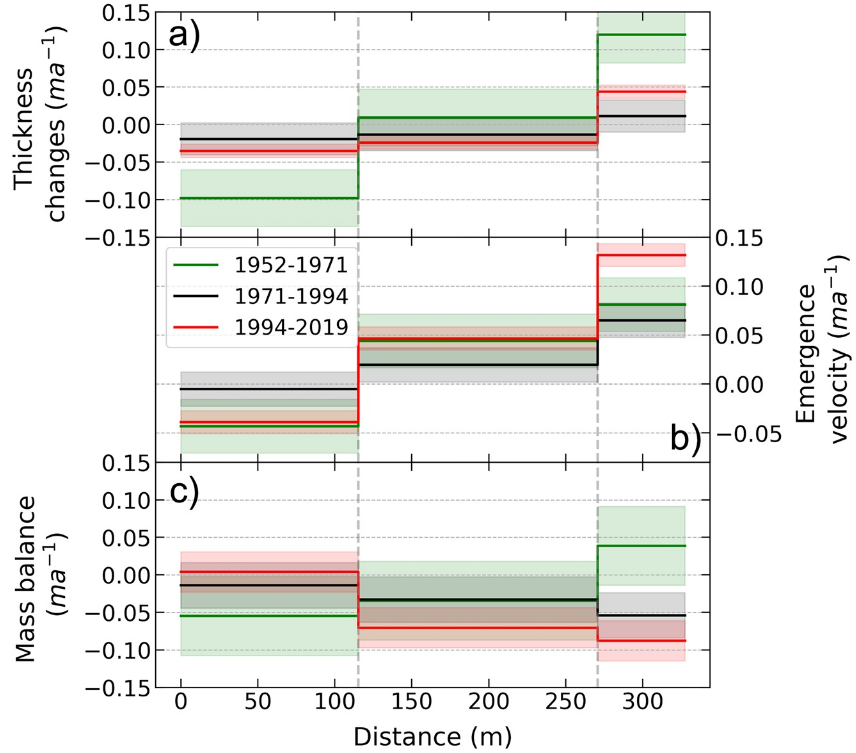

Figure 7. (a) Changes in thickness (m a^{-1}), (b) emergence velocities (m a^{-1}), and (c) surface mass balances (m a^{-1}) for the three subperiods (1952–1971, 1971–1994, and 1994–2019) and three sectors (PT10-PT7, PT7-PT3, and PT3-PT1). The colored rectangles correspond to the uncertainty estimated after uncertainty propagation analysis (Equation 5).

Considering the uncertainties in the quantified mass balances, the shift in surface mass balance gradient appears to be significant. This is discussed in the following section.

5. Discussion

The reconstruction of the surface mass balance of the Laurichard rock glacier provides interesting and original insights into the complex behavior of such landforms. Although little is known about the mechanisms that drive inputs of debris and ice in rock glaciers or the melting rates inside rock glaciers, here we discuss possible hypotheses to explain the results obtained at Laurichard.

5.1. Altitudinal Gradient of Surface Mass Balance

The reconstructed surface mass balance of the rock glacier for the period 1952–1971 includes one striking feature, that is, more negative values in the upper part than in the tongue. Because the oldest DSMs are less accurate, caution is called for when interpreting the values during this period than the values of more recent periods; we propose two hypotheses to explain the negative surface mass balance in the upper part of the rock glacier.

The first hypothesis concerns the accumulation of snow. Although snowfall assessed using meteorological data revealed no important changes over this period (Figure 2), some authors have reported that the regional avalanche activity was lower during the period ∼1955–1970 (Naaim et al., 2016) and in parallel, that the lowest altitudes reached by the avalanches were higher. This suggests that less snow may have accumulated at the surface of the rock glacier, compared to the following subperiods, leading to the observed lower surface mass balance.

The second hypothesis concerns variations in rock falls onto the surface of the rock glacier from the dominating rock wall named *"Roc Noir de Combeynot."* Indeed, according to the results of several numerical modeling experiments of frost cracking simulating both volumetric expansion and ice segregation (Draebing & Krautblatter, 2019; Hales & Roering, 2007), colder temperatures in the decade 1950–1960 could have kept the rock wall frozen at low enough temperatures to prevent large rock falls (Hales & Roering, 2007). In this case, the negative surface mass balance would be explained by a deficit of debris accumulation. This hypothesis is supported by colder air temperatures recorded during the first period (1952–1971): The mean positive daily temperature increased from 0.3°C to 0.7°C between the first two periods (1952–1971 and 1971–1994) and the third period (1994–2019). Higher rockfall from frozen rock walls recorded in the Alps also increased during the recent warmer period (Huggel et al., 2012; Ravanel & Deline, 2011; Ravanel et al., 2017).

The positive surface mass balance in the lowest sector over the period 1952–1971 is more problematic, it cannot be explained by an increase in debris accumulation as this region is located far from the rock wall and is not impacted by rockfall. Regarding the balance of the ice component, it is known that Alpine glacier melting rates were reduced during the period 1952–1971 (Huss et al., 2010; Vincent, 2002). Given the large uncertainty on the estimated value, one can therefore hypothesize that ice melt inside the rock glacier was close to zero at this altitude over this period.

Over the following periods, the reconstructed surface mass balance returned to the usual pattern with a positive altitudinal gradient. In the last period (1994–2019), the surface mass balance decreased slightly particularly in the lower sector to reach -0.10 m a^{-1}. This period corresponds to marked climate warming (Figure 2) and hence, an important increase in glacier ice melt throughout the Alps (Davaze et al., 2020). At Laurichard, ice melt was clearly very low compared to that observed in surrounding glaciers where the surface mass balance dropped by several meters over the period (Vincent et al., 2017) versus a few centimeters of thawing that affected the tongue of the Laurichard rock glacier. However, inside the rock glacier, the ice is covered by a thick layer of debris that acts as a strong insulator and consequently damping melt (e.g., Anderson et al., 2018; Evatt et al., 2015; Hoelzle et al., 2001; Jones et al., 2019; Pruessner, 2017).

5.2. Influence of Internal Accumulation and Internal Ablation on Surface Mass Balance Assessment

As mentioned previously, the reconstructed surface mass balances obtained from the emergence velocities and the thickness did not account for internal accumulation and internal ablation.

Internal accumulation can occur when the water that percolates into the rock glacier freezes when it comes into contact with massive ice or rocks at negative temperatures. Because these phenomena are still poorly understood in rock glaciers, internal accumulation was calculated following Trabant and Mayo (1985) and Thibert et al. (2008) assuming that cold internal conditions exist inside the rock glacier. Relying on the studies by Gerbaux et al. (2005) on Saint-Sorlin Glacier, we considered a mean sensible heat flux of 5,000 kJ m^{-2} that cools the snowpack during winter. This value was estimated using the *Crocus* snow model (Brun et al., 1989). In addition, we used a specific latent heat of fusion of 335 kJ Kg^{-1} (Hobbs, 1974). This gave an internal accumulation of 5.6 mm a^{-1}, thus accounting for 37 cm over the 67-year study period. Considering the uncertainties on the reconstructed surface mass balance, this accumulation can be disregarded.

The internal ablation of the ice inside the rock glacier can be linked to different sources of energy: (a) geothermal heat; (b) conversion into heat of energy lost from water originating from snowmelt at the surface of the rock glacier or from summer rainfall flowing through and under the glacier; and (c) the change in air convection within the coarse blocky layer associated with a change in the temperature gradients due to a change in the temperature of the air above the surface of the rock glacier and the permeability in the active layer. According to Gable and Goguel (1981), a maximum value of ~90 mW m^{-2} of the geothermal flux can be considered in this part of the Alps; this results in a maximum value of basal melting of 9 mm a^{-1}. Regarding ablation from water flow, March and Trabant (1997) described their principle of calculation related to two main sources. The first is runoff originating from the 0.14 km^2 catchment above the rock glacier. If we assume that the winter snowpack in this part of the catchment melts completely in summer and that all the melt water circulates at the base of the rock glacier, this would result in 7 mm a^{-1} of ice melt due to the conversion of the potential energy loss of this water flow into heat. The second source of energy is water flow from the melting of the rock glacier itself (over an area of 0.07 km^2), which would account for only 1 cm over the 67 years and can therefore be disregarded. Regarding the energy related to air convec-

10.1029/2021JF006161

tion, Wicky and Hauck (2020) showed that this process would only be efficient if both permeability and the temperature gradient are high in the upper blocky layer that covers the ice-rich core of rock glaciers. Note that although air convection has a cooling effect, it has limited impact on the mass balance. The theoretical approach presented by Evatt et al. (2015) already underlined the role of the porosity of the debris layer in modulating the melt process under the debris.

To sum up, both internal accumulation and ablation seem to play a negligible role in the changes in volume and mass in Laurichard. This gives us confidence in the approach we used to quantify changes from observations at the rock glacier surface (elevation, velocities) to retrieve the surface mass balance from the emergence velocity (Equation 4).

5.3. Acceleration of Flow

Another important feature of the behavior of this rock glacier is the marked increase in flow velocities over the most recent period (1994–2019). This acceleration has been visible in in-situ observations since the 1990s (Figure 5) (Bodin et al., 2009; Thibert et al., 2018). Similar acceleration has been reported in many rock glaciers in the Alps (Delaloye et al., 2008, 2018) as well as in other mountain chains in the world (e.g., Kääb et al., 2021; Sorg et al., 2015). Several hypotheses have been proposed to explain this acceleration: (a) the change in rheological properties and internal temperatures with an impact on the viscosity and rheology (Cicoira et al., 2021; Müller et al., 2016); (b) the influence of water percolation (likely down to the shear horizon), originating from snow melt in spring (Buchli et al., 2018; Cicoira, Beutel, Faillettaz, Gärtner-Roer, & Vieli, 2019; Kenner et al., 2017; Wirz et al., 2016) but also from ice melt (Bodin et al., 2009); or (c) a change in basal thermal conditions (at the shear horizon) that could cause basal melting and affects the mechanical properties of the rock glacier material (Cicoira et al., 2021; Haeberli et al., 1998).

Our observations do not enable us to solve this issue but lead to several hypotheses. Indeed, our results show that, given the only slight changes we observed over this period, the acceleration cannot be explained by changes in geometry (thickness and slope) and surface mass balance. What is more, the acceleration is not consistent with thinning in the upper part of the rock glacier which would reduce creep. For instance, applying again the Glen's (1955) flow law to relate changes in flow and changes in geometry using a realistic set of parameters (based on observations) does not give consistent results. As an illustration, considering the middle part of Laurichard rock glacier, the surface slope and the averaged thickness between 1952 and 2019 has changed from 32° to 36° and 20 to 19 m, respectively. Keeping other parameters constant in Glen's law gives a change in velocity from 0.6 to 0.5 m a^{-1}, which is not consistent with the observed increase (from 0.8 to 1.1 m a^{-1}). One can thus conclude that the increase in velocity is very likely caused by internal changes or/and basal conditions.

As a first explanation, as mentioned by Cicoira, Beutel, Faillettaz, Gärtner-Roer and Vieli (2019), Cicoira et al. (2021), the process of heat conduction alone cannot explain the observed variations in surface velocity, except in thin rock glaciers (less than 20 m thick according to Cicoira, Beutel, Faillettaz, Gärtner-Roer, & Vieli, 2019) that are more sensitive to the effect of heat conduction on seasonal as well as long-term temperature changes. However, it is possible that the indirect effect of enhanced meltwater penetrating the rock glacier body thereby affecting its rheology plays a role. Then, regarding the possibility that a change in viscosity related to a change in internal temperature could explain the observed acceleration, if we assume that the internal structure is composed of pure ice (below the debris cover) and a cold thermal regime at the beginning of the study period (e.g., an ice temperature of −5°C in the 1950s), applying the Glen's (1955) flow law shows that a 3°C increase in temperature within the rock glacier would be required to explain a change in viscosity leading to a doubling of the ice flow velocity (Glen, 1955). This is a large increase given that the englacial temperatures recorded at Murtèl rock glacier (∼300 km away, 2,670 m a.s.l., northern exposure, Engadine, Swiss Alps) only increased from −1.8°C to −1.1°C between 1988 and 2015 at a depth of 10 m (Cicoira, Beutel, Faillettaz, Gärtner-Roer, & Vieli, 2019; PERMOS, 2019). Despite the absence of any information about the ice content and the internal temperature in the Laurichard rock glacier, this assumption can almost certainly be ruled out as air temperature showed no such increase in recent decades (Figure 2), and because warming of the ice inside a rock glacier requires a long time (e.g., several decades; PERMOS, 2019). Numerical modeling would be required to estimate the time necessary to modify the thermal regime at depth, which is beyond the scope of the present study.

Thus, the change in the conditions in the shear layer and at the base (in terms of thermal regime, presence of water) related to basal temperate conditions reached at the beginning of the 1990s is a good candidate to explain the accelerated rock glacier flow (Cicoira et al., 2021). Unfortunately, no borehole data are available for Laurichard rock glacier, but this hypothesis is supported by the availability of water through snow melt, which since the 1990s has started earlier in the season. Today water is released into the rock glacier a month earlier than in the former periods (Figure S7). Such changes in the shear layer and at the base could also explain why the increase in velocity is homogeneous over the entire landform whatever the slope and thickness as observed in 1980–2020 topographic surveys (Thibert et al., 2018).

6. Conclusions

The measurements we made from aerial photographs using photogrammetry and feature -tracking image correlation techniques allowed us to identify changes in decadal thickness, velocities, and fluxes over the period 1952–2019. From these data sets, emergence velocities and surface mass balance of a rock glacier have been reconstructed for the first time. Our reconstruction revealed a very small surface mass balance ranging from -0.1 to $+0.05$ m a^{-1} compared to those obtained on glaciers at similar altitudes; the average mass balance on regional glaciers at similar elevations (2,500 m a.s.l.) with northern exposure has been about -5 m w.e. a^{-1} over recent decades (e.g., Six & Vincent, 2014; Vincent et al., 2017). It will be recalled that in the present study, the surface mass balances are expressed in m a^{-1} (and not m w.e. a^{-1}) as they concern changes in net ice and/or in rock mass.

We identified three periods during which the fluctuations were homogeneous, and we analyzed them in three selected regions of the rock glacier. The first period, characterized by colder air temperatures, had a low surface mass balance in the upper part of the rock glacier, which could be linked to reduced rock falls and snow avalanches. In contrast, the surface mass balance in the lower part was close to zero, likely explained by reduced melting, resulting in a striking negative altitudinal balance gradient. Over the following periods, the surface mass balance of the upper region again reached values close to zero, suggesting an increase in rock fall. This reversal of the altitudinal balance gradient could appear paradoxical. Indeed, the surface mass balance was negative (positive) in the upper region during the cold (warm) period. The emergence velocities remained very even over the whole period except in the lower region in the most recent period, the latter could be explained by the compressive flow related to the advance of the terminus and the hypothesis of incompressible material, which is true for ice but not for debris, or for a mixture of ice and debris.

As a result of our study, we are able to explain the changes in thickness by the emergence velocities and surface mass balance. Between 1952 and 1971, the thinning (thickening) of the upper (lower) region was due to the decrease (increase) in the surface mass balance. Between 1971 and 1994, the surface mass balance almost compensated for the emergence velocities and the changes in thickness were small. Between 1994 and 2019, the increase in rockfalls led to an increase in the surface mass balance, which balances the emergence velocities and explains the limited changes in thickness in the upper part of the rock glacier. Conversely, in the lower part, the negative surface mass balance likely cannot compensate for the increase in emergence velocity due to compressive flow.

Finally, our observations revealed a marked increase in flow velocities over the period 1994–2019. Surprisingly, it affected the fluxes but had no clear effect on the emergence velocities, thereby supporting the hypothesis that the surface mass balance mainly controls changes in thickness, except in the lower part of the rock glacier in the most recent period. On the other hand, changes in geometry did not affect flow velocities. Indeed, the marked acceleration after 1994 was accompanied by the thinning of a large part of the rock glacier, leading us to propose the hypothesis that the increase in velocity was very likely caused by changes in the conditions in the shear layer and at the base (in terms of thermal regime and the presence of water) related to the basal temperate conditions reached at the beginning of the 1990s. This hypothesis is strengthened by the homogeneity of the increase in velocity throughout the rock glacier whatever the slope and thickness.

In this sense, sub-annual resolution time series from continuous dGNSS measurements as made by Cicoira, Beutel, Faillettaz, Gärtner-Roer, and Vieli (2019) or terrestrial daily photogrammetric measurements (Marsy et al., 2020) could help to detect the role of changes in basal conditions in the rock glacier flow. Additionally, numerical modeling will help test the validity of the basal conditions hypothesis, however, due to the complexity of the rock glacier, further geo-mechanical observations of the internal structure and its spatial distribution are also needed.

Conflict of Interest

The authors declare no conflicts of interest relevant to this study.

Data Availability Statement

Main data supporting the findings of this study could be accessed through the Pangea data repository (https://doi.pangaea.de/10.1594/PANGAEA.932315). This data set includes raw DSM's, surface velocities computed for different periods and multi-temporal rock glacier animations. Yearly GNSS measurements of Laurichard rock glacier can be seen in Bodin et al. (2009) and Thibert et al. (2018) (https://doi.org/10.1002/ppp.665).

Acknowledgments
This work was supported by the French National Research Agency in the framework of the *Investissements d'Avenir* programs: Risk@UGA (ANR-15-IDEX-02) and LabEx OSUG@2020 (ANR10 LABX56). This study is also part of the PERMARISK project, funded by the European Regional Development Fund (grant POIA PA0004100). The Jardin Alpin du Lautaret (CNRS/Univ. Grenoble Alpes) provided support and facilities for fieldwork as well as the 2012 aerial LiDAR survey. Surface velocity measurements were started by B. Francou and L. Reynaud and continued by E. Thibert (Ecrins National Park and later ETNA, INRAe-UGA), and since 2001, by M. Bouvier (Ecrins National Park). The last two decades of the survey were supported by CryobsClim "Long-term Observation and Experimentation System for Environmental Research" (SOERE/All'envi) and the PermaFrance observatory that monitors mountain permafrost in the French Alps. The Ecrins National Park is sincerely acknowledged for funding and supporting field surveys since the early 2000s. We are grateful to Michael Deschatres, Sylvain Pech, and Guilhem Marsy for field campaigns and to Antoine Guillemot and Stéphane Garambois for the GPR data, and to Olivier Gagliardini for discussions on ice dynamics. Finally, we thank Robert Anderson and the two anonymous reviewers whose comments and suggestions greatly helped to improve and clarify this manuscript.

References

Abermann, J., Fischer, A., Lambrecht, A., & Geist, T. (2010). On the potential of very high-resolution, repeat DEMs in glacial and periglacial environments. *The Cryosphere*, *4*(1), 53–65. https://doi.org/10.5194/tc-4-53-2010

Anderson, L. S., & Anderson, R. S. (2016). Modeling debris-covered glaciers: Response to steady debris deposition. *The Cryosphere*, *10*(3), 1105–1124. https://doi.org/10.5194/tc-10-1105-2016

Anderson, R. S., Anderson, L. S., Armstrong, W. H., Rossi, M. W., & Crump, S. E. (2018). Glaciation of alpine valleys: The glacier – debris-covered glacier – rock glacier continuum. *Geomorphology*, *311*, 127–142. https://doi.org/10.1016/j.geomorph.2018.03.015

Arenson, L., Hoelzle, M., & Springman, S. (2002). Borehole deformation measurements and internal structure of some rock glaciers in Switzerland. *Permafrost and Periglacial Processes*, *13*(2), 117–135. https://doi.org/10.1002/ppp.414

Arenson, L. U., & Springman, S. M. (2005). Mathematical descriptions for the behaviour of ice-rich frozen soils at temperatures close to 0°C. *Canadian Geotechnical Journal*, *42*(2), 431–442. https://doi.org/10.1139/t04-109

Barsch, D. (1996). *Rock glaciers. Indicators for the present and former geoecology in high mountain environments* (p. 331). Springer-Verlag Berlin Heidelberg Springer Series in Physical Environment. https://doi.org/10.1007/978-3-642-80093-1

Beniston, M., Farinotti, D., Stoffel, M., Andreassen, L. M., Coppola, E., Eckert, N., et al. (2018). The European mountain cryosphere: A review of its current state, trends, and future challenges. *The Cryosphere*, *12*(2), 759–794. https://doi.org/10.5194/tc-12-759-2018

Bodin, X., Thibert, E., Fabre, D., Ribolini, A., Schoeneich, P., Francou, B., et al. (2009). Two decades of responses (1986–2006) to climate by the Laurichard rock glacier, French Alps. *Permafrost and Periglacial Processes*, *20*(4), 331–344. https://doi.org/10.1002/ppp.665

Bodin, X., Thibert, E., Sanchez, O., Rabatel, A., & Jaillet, S. (2018). Multi-annual kinematics of an active rock glacier quantified from very high-resolution DEMs: An application-case in the french alps. *Remote Sensing*, *10*(4), 547. https://doi.org/10.3390/rs10040547

Bollmann, E., Girstmair, A., Mitterer, S., Krainer, K., Sailer, R., & Stötter, J. (2015). A rock glacier activity index based on rock glacier thickness changes and displacement rates derived from airborne laser scanning. *Permafrost and Periglacial Processes*, *26*(4), 347–359. https://doi.org/10.1002/ppp.1852

Brun, E., Martin, E., Simon, V., Gendre, C., & Coleou, C. (1989). An energy and mass model of snow cover suitable for operational avalanche forecasting. *Journal of Glaciology*, *35*(121), 333–342. https://doi.org/10.3189/S0022143000009254

Buchli, T., Kos, A., Limpach, P., Merz, K., Zhou, X., & Springman, S. M. (2018). Kinematic investigations on the Furggwanghorn Rock Glacier, Switzerland. *Permafrost and Periglacial Processes*, *29*(1), 3–20. https://doi.org/10.1002/ppp.1968

Cicoira, A., Beutel, J., Faillettaz, J., Gärtner-Roer, I., & Vieli, A. (2019). Resolving the influence of temperature forcing through heat conduction on rock glacier dynamics: A numerical modelling approach. *The Cryosphere*, *13*(3), 927–942. https://doi.org/10.5194/tc-13-927-2019

Cicoira, A., Beutel, J., Faillettaz, J., & Vieli, A. (2019). Water controls the seasonal rhythm of rock glacier flow. *Earth and Planetary Science Letters*, *528*, 115844. https://doi.org/10.1016/j.epsl.2019.115844

Cicoira, A., Marcer, M., Gärtner-Roer, I., Bodin, X., Arenson, L. U., & Vieli, A. (2021). A general theory of rock glacier creep based on in-situ and remote sensing observations. *Permafrost and Periglacial Processes*, *32*, 139–153. https://doi.org/10.1002/ppp.2090

Cogley, J. G., Hock, R., Rasmussen, L. A., Arendt, A. A., Bauder, A., Jansson, P., et al. (2011). *Glossary of glacier mass balance related terms*. IHP-VII Technical Documents in Hydrology (IACS Contribution No. 2). (Vol. 86, p. 144). UNESCO-IHP.

Conrad, O., Bechtel, B., Bock, M., Dietrich, H., Fischer, E., Gerlitz, L., et al. (2015). System for automated geoscientific analyses (SAGA) v. 2.1.4. *Geoscientific Model Development Discussions*, *8*, 2271–2312. https://doi.org/10.5194/gmdd-8-2271-2015

Coutard, J.-P., & Francou, B. (1989). Rock temperature measurements in two alpine environments: Implications for frost shattering. *Arctic and Alpine Research*, *21*(4), 399–416. https://doi.org/10.1080/00040851.1989.12002753

Cuffey, K., & Paterson, W. S. B. (2010). *The physics of glaciers* (4th ed.). Retrieved from https://www.elsevier.com/books/the-physics-of-glaciers/cuffey/978-0-12-369461-4

Davaze, L., Rabatel, A., Dufour, A., Hugonnet, R., & Arnaud, Y. (2020). Region-wide annual glacier surface mass balance for the European Alps from 2000 to 2016. *Frontiers of Earth Science*, *8*, 149. https://doi.org/10.3389/feart.2020.00149

Delaloye, R., Barboux, C., Bodin, X., Brenning, A., Hartl, L., Hu, Y., & Ikeda, A. (2018). Rock glacier inventories and kinematics: A new IPA Action Group. In *5th European Conference on Permafrost, Book of Abstract* (pp. 392–393). Chamonix, France. Laboratoire EDYTEM.

Delaloye, R., Lambiel, C., & Gärtner-Roer, I. (2010). Overview of rock glacier kinematics research in the Swiss Alps. Seasonal rhythm, interannual variations and trends over several decades. *Geographica Helvetica*, *65*(2), 135–145. https://doi.org/10.5194/gh-65-135-2010

Delaloye, R., Perruchoud, E., Avian, M., Kaufmann, V., Bodin, X., Hausmann, H., et al. (2008). Recent interannual variations of rock glacier creep in the European Alps. (pp. 343–348). Presented at the 9th International Conference on Permafrost 29 June 2008–3 July 2008, Fairbanks, Alaska.

Deline, P., Gruber, S., Delaloye, R., Fischer, L., Geertsema, M., Giardino, M., et al. (2015). Chapter 15 - Ice loss and slope stability in high-mountain regions. In J. F. Shroder, W. Haeberli, & C. Whiteman (Eds.), *Snow and ice-related hazards, risks and disasters* (pp. 521–561). Boston. Academic Press. https://doi.org/10.1016/B978-0-12-394849-6.00015-9

Draebing, D., & Krautblatter, M. (2019). The efficacy of frost weathering processes in alpine rockwalls. *Geophysical Research Letters*, *46*(12), 6516–6524. https://doi.org/10.1029/2019GL081981

Durand, Y., Giraud, G., Laternser, M., Etchevers, P., Mérindol, L., & Lesaffre, B. (2009). Reanalysis of 47 years of climate in the French Alps (1958–2005): Climatology and trends for snow cover. *Journal of Applied Meteorology and Climatology*, *48*(12), 2487–2512. https://doi.org/10.1175/2009JAMC1810.1

Durand, Y., Laternser, M., Giraud, G., Etchevers, P., Lesaffre, B., & Mérindol, L. (2009). Reanalysis of 44 Yr of climate in the French Alps (1958–2002): Methodology, model validation, climatology, and trends for air temperature and precipitation. *Journal of Applied Meteorology and Climatology*, *48*(3), 429–449. https://doi.org/10.1175/2008JAMC1808.1

Duvillard, P.-A., Ravanel, L., Marcer, M., & Schoeneich, P. (2019). Recent evolution of damage to infrastructure on permafrost in the French Alps. *Regional Environmental Change*, *19*(5), 1281–1293. https://doi.org/10.1007/s10113-019-01465-z

Dyurgerov, M. B., & Meier, M. F. (2000). Twentieth century climate change: Evidence from small glaciers. *Proceedings of the National Academy of Sciences of the United States of America*, *97*(4), 1406–1411. https://doi.org/10.1073/pnas.97.4.1406

Eriksen, H. Ø., Rouyet, L., Lauknes, T. R., Berthling, I., Isaksen, K., Hindberg, H., et al. (2018). Recent acceleration of a rock glacier complex, Ádjet, Norway, documented by 62 years of remote sensing observations. *Geophysical Research Letters*, *45*, 8314–8323. https://doi.org/10.1029/2018GL077605

Evatt, G. W., Abrahams, I. D., Heil, M., Mayer, C., Kingslake, J., Mitchell, S. L., & Fowler, C. D. (2015). Glacial melt under a porous debris layer. *Journal of Glaciology*, *61*(229), 825–836. https://doi.org/10.3189/2015jog14j235

Francou, B., & Reynaud, L. (1992). 10 year surficial velocities on a rock glacier (Laurichard, French Alps). *Permafrost and Periglacial Processes*, *3*(3), 209–213. https://doi.org/10.1002/ppp.3430030306

Frehner, M., Ling, A. H. M., & Gärtner-Roer, I. (2015). Furrow-and-ridge morphology on rock glaciers explained by gravity-driven buckle folding: A case study from the Murtèl Rockglacier (Switzerland). *Permafrost and Periglacial Processes*, *26*(1), 57–66. https://doi.org/10.1002/ppp.1831

Gable, R., & Goguel, J. (1981). Carte du flux géothermique. In P. Souquet (Ed.), *Structure et dynamique de la lithosphe`re* (Vol. 2). Toulouse. Centre Régional de Documentation Pédagogique de Midi-Pyrénées.

Gerbaux, M., Genthon, C., Etchevers, P., Vincent, C., & Dedieu, J. P. (2005). Surface mass balance of glaciers in the French Alps: Distributed modeling and sensitivity to climate change. *Journal of Glaciology*, *51*(175), 561–572. https://doi.org/10.3189/172756505781829133

Giardino, J. R., Regmi, N. R., & Vitek, J. D. (1987). Rock glaciers. In V. P. Singh, P. Singh, & U. K. Haritashya (Eds.), *Encyclopedia of snow, ice and glaciers* (pp. 943–948). Dordrecht. Springer Netherlands. https://doi.org/10.1007/978-90-481-2642-2_453

Glen, J. W. (1955). The creep of polycrystalline ice. *Proceedings of the Royal Society of London - Series A: Mathematical and Physical Sciences*, *228*(1175), 519–538. https://doi.org/10.1098/rspa.1955.0066

Goetz, J., Fieguth, P., Kasiri, K., Bodin, X., Marcer, M., & Brenning, A. (2019). Accounting for permafrost creep in high-resolution snow depth mapping by modelling sub-snow ground deformation. *Remote Sensing of Environment*, *231*, 111275. https://doi.org/10.1016/j.rse.2019.111275

Gruber, S., & Ludwig, F. (1996). *Application of ground penetrating radar in glaciology and permafrost Prospecting*. Lapland. Arctic Center, University of Lapland. Retrieved from http://www.ulapland.fi/home/hkunta/jmoore/gpr_cryo.pdf

Guillemot, A., Baillet, L., Garambois, S., Bodin, X., Helmstetter, A., Mayoraz, R., & Larose, E. (2021). Modal sensitivity of rock glaciers to elastic changes from spectral seismic noise monitoring and modeling. *The Cryosphere*, *15*, 501–529. https://doi.org/10.5194/tc-15-501-2021

Haeberli, W. (1985). Creep of mountain permafrost: Internal structure and flow of alpine rock glaciers. *Mitteilungen der Versuchsanstalt für Wasserbau Hydrologie und Glaziologie an der Eidgenössischen Technischen Hochschule Zürich*, vol. *77*, Zürich. 142 pp.

Haeberli, W., Guodong, C., Gorbunov, A. P., & Harris, S. A. (1993). Mountain permafrost and climatic change. *Permafrost and Periglacial Processes*, *4*(2), 165–174. https://doi.org/10.1002/ppp.3430040208

Haeberli, W., Hallet, B., Arenson, L., Elconin, R., Humlum, O., Kääb, A., et al. (2006). Permafrost creep and rock glacier dynamics. *Permafrost and Periglacial Processes*, *17*(3), 189–214. https://doi.org/10.1002/ppp.561

Haeberli, W., Hoelzle, M., Kääb, A., Keller, F., Vonder, D. V., & Wagner, S. (1998). Ten years after drilling through the permafrost of the active rock glacier Murtél, eastern Swiss Alps: Answered questions and new perspectives. *Proceedings of the PERMAFROST - Seventh International Conference*, 55, 8.

Haeberli, W., Noetzli, J., Arenson, L., Delaloye, R., Gärtner-Roer, I., Gruber, S., et al. (2010). Mountain permafrost: Development and challenges of a young research field. *Journal of Glaciology*, *56*(200), 1043–1058. https://doi.org/10.3189/002214311796406121

Hales, T. C., & Roering, J. J. (2007). Climatic controls on frost cracking and implications for the evolution of bedrock landscapes. *Journal of Geophysical Research*, *112*(F2), F02033. https://doi.org/10.1029/2006JF000616

Harris, C., Davies, M. C. R., & Etzelmüller, B. (2001). The assessment of potential geotechnical hazards associated with mountain permafrost in a warming global climate. *Permafrost and Periglacial Processes*, *12*(1), 145–156. https://doi.org/10.1002/ppp.376

Hartl, L., Fischer, A., Stocker-Waldhuber, M., & Abermann, J. (2016). Recent speed-up of an Alpine rock glacier: An updated chronology of the kinematics of Outer Hochebenkar rock glacier based on geodetic measurements. *Geografiska Annaler - Series A: Physical Geography*, *98*, 129–141. https://doi.org/10.1111/geoa.12127

Hobbs, P. V. (1974). *Ice physics*, xvii (p. 837). Oxford. Clarendon Press.

Hock, R., Rasul, G., Adler, C., Cceres, B., Gruber, S., Hirabayashi, Y., et al. (2019). High mountain areas. In H.-O. Prtner, D. C. Roberts, V. Masson-Delmotte, P. Zhai, M. Tignor, et al. (Eds.), *Special report on the ocean and cryosphere in a changing climate: IPCC*. Retrieved from https://www.ipcc.ch/srocc/chapter/chapter-2/

Hoelzle, M., Mittaz, C., Etzelmüller, B., & Haeberli, W. (2001). Surface energy fluxes and distribution models of permafrost in European mountain areas: An overview of current developments. *Permafrost and Periglacial Processes*, *12*(1), 53–68. https://doi.org/10.1002/ppp.385

Huggel, C., Carey, M., Clague, J. J., & Kääb, A. (2015). *The high-mountain cryosphere: Environmental changes and human risks*. Cambridge. Cambridge University Press. https://doi.org/10.1017/CBO9781107588653

Huggel, C., Clague, J. J., & Korup, O. (2012). Is climate change responsible for changing landslide activity in high mountains? *Earth Surface Processes and Landforms*, *37*(1), 77–91. https://doi.org/10.1002/esp.2223

Huss, M. (2012). Extrapolating glacier mass balance to the mountain-range scale: The European Alps 1900–2100. *The Cryosphere*, *6*(4), 713–727. https://doi.org/10.5194/tc-6-713-2012

Huss, M., Bookhagen, B., Huggel, C., Jacobsen, D., Bradley, R. S., Clague, J. J., et al. (2017). Toward mountains without permanent snow and ice. *Earth's Future*, *5*(5), 418–435. https://doi.org/10.1002/2016EF000514

Huss, M., Hock, R., Bauder, A., & Funk, M. (2010). 100-year mass changes in the Swiss Alps linked to the Atlantic Multidecadal Oscillation. *Geophysical Research Letters*, *37*(10), L10501. https://doi.org/10.1029/2010GL042616

Jansen, F., & Hergarten, S. (2006). Rock glacier dynamics: Stick-slip motion coupled to hydrology. *Geophysical Research Letters*, *33*(10), L10502. https://doi.org/10.1029/2006GL026134

Jol, H. M., & Bristow, C. S. (2003). GPR in sediments: Advice on data collection, basic processing and interpretation, a good practice guide. *Geological Society, London, Special Publications*, *211*(1), 9–27. https://doi.org/10.1144/GSL.SP.2001.211.01.02

Jomelli, V., & Francou, B. (2000). Comparing the characteristics of rockfall talus and snow avalanche landforms in an Alpine environment using a new methodological approach: Massif des Ecrins, French Alps. *Geomorphology*, *35*, 181–192. https://doi.org/10.1016/S0169-555X(00)00035-0

Jones, D. B., Harrison, S., Anderson, K., & Whalley, W. B. (2019). Rock glaciers and mountain hydrology: A review. *Earth-Science Reviews*, *193*, 66–90. https://doi.org/10.1016/j.earscirev.2019.04.001

Kääb, A., Frauenfelder, R., & Roer, I. (2007). On the response of rockglacier creep to surface temperature increase. *Global and Planetary Change*, *56*(1–2), 172–187. https://doi.org/10.1016/j.gloplacha.2006.07.005

Kääb, A., Haeberli, W., & Gudmundsson, G. H. (1997). Analysing the creep of mountain permafrost using high precision aerial photogrammetry: 25 years of monitoring Gruben rock glacier, Swiss Alps. *Permafrost and Periglacial Processes*, *8*(4), 409–426. https://doi.org/10.1002/(SICI)1099-1530(199710/12)8:4<409::AID-PPP267>3.0.CO;2-C

Kääb, A., Strozzi, T., Bolch, T., Caduff, R., Trefall, H., Stoffel, M., & Kokarev, A. (2021). Inventory, motion and acceleration of rock glaciers in Ile Alatau and Kungöy Ala-Too, northern Tien Shan, since the 1950s. *The Cryosphere*, *15*, 927–949. https://doi.org/10.5194/tc-15-927-2021

Kellerer-Pirklbauer, A., Delaloye, R., Lambiel, C., Gärtner-Roer, I., Kaufmann, V., Scapozza, C., et al. (2018). Interannual variability of rock glacier flow velocities in the European Alps. In. *5th European Conference on Permafrost, June 2018, Chamonix, France, Book of Abstract, Edytem* (pp. 396–397). Chamonix.

Kenner, R., Phillips, M., Beutel, J., Hiller, M., Limpach, P., Pointner, E., & Volken, M. (2017). Factors controlling velocity variations at short-term, seasonal and multiyear time scales, Ritigraben rock glacier, Western Swiss Alps. *Permafrost and Periglacial Processes*, *28*(4), 675–684. https://doi.org/10.1002/ppp.1953

Kenner, R., Pruessner, L., Beutel, J., Limpach, P., & Phillips, M. (2019). How rock glacier hydrology, deformation velocities and ground temperatures interact: Examples from the Swiss Alps. *Permafrost and Periglacial Processes*, *31*(1), 3–14. https://doi.org/10.1002/ppp.2023

Marcer, M., Bodin, X., Brenning, A., Schoeneich, P., Charvet, R., & Gottardi, F. (2017). Permafrost favorability index: Spatial modeling in the French Alps using a rock glacier inventory. *Frontiers of Earth Science*, *5*, 105. https://doi.org/10.3389/feart.2017.00105

Marcer, M., Cicoira, A., Cusicanqui, D., Bodin, X., Echelard, T., Obregon, R., & Schoeneich, P. (2021). Rock glaciers throughout the French Alps accelerated and destabilised since 1990 as air temperatures increased. *Nature Communications Earth & Environment*, *2*, 1–11. https://doi.org/10.1038/s43247-021-00150-6

Marcer, M., Nielsen, S. R., Ribeyre, C., Kummert, M., Duvillard, P.-A., Schoeneich, P., et al. (2020). Investigating the slope failures at the Lou rock glacier front, French Alps. *Permafrost and Periglacial Processes*, *31*(1), 15–30. https://doi.org/10.1002/ppp.2035

March, R. S., & Trabant, D. C. (1997). *Mass balance, meteorological, ice motion, surface altitude, and runoff data at Gulkana Glacier, Alaska, 1993 balance year*. USGS Water-Resources Investigations Reports, 96–4299.

Marmy, A., Rajczak, J., Delaloye, R., Hilbich, C., Hoelzle, M., Kotlarski, S., et al. (2016). Semi-automated calibration method for modelling of mountain permafrost evolution in Switzerland. *The Cryosphere*, *10*, 2693–2719. https://doi.org/10.5194/tc-10-2693-2016

Marsy, G., Vernier, F., Bodin, X., Cusicanqui, D., Castaings, W., & Trouvé, E. (2020). Monitoring mountain cryosphere dynamics by time lapse stereo photogrammetry. In *ISPRS Annals of the Photogrammetry, Remote Sensing and Spatial Information Sciences* (Vol. V-2–2020, pp. 459–466). Copernicus GmbH. https://doi.org/10.5194/isprs-annals-V-2-2020-459-2020

Mellor, M., & Testa, R. (1969). Effect of temperature on the creep of ice. *Journal of Glaciology*, *8*(52), 131–145. https://doi.org/10.3189/S0022143000020803

Mertes, J. R., Gulley, J. D., Benn, D. I., Thompson, S. S., & Nicholson, L. I. (2017). Using structure-from-motion to create glacier DEMs and orthoimagery from historical terrestrial and oblique aerial imagery. *Earth Surface Processes and Landforms*, *42*(14), 2350–2364. https://doi.org/10.1002/esp.4188

Micheletti, N., Lane, S. N., & Chandler, J. H. (2015). Application of archival aerial photogrammetry to quantify climate forcing of alpine landscapes. *The Photogrammetric Record*, *30*(150), 143–165. https://doi.org/10.1111/phor.12099

Mölg, N., & Bolch, T. (2017). Structure-from-motion using historical aerial images to analyse changes in glacier surface elevation. *Remote Sensing*, *9*(10), 1021. https://doi.org/10.3390/rs9101021

Mollaret, C., Hilbich, C., Pellet, C., Flores-Orozco, A., Delaloye, R., & Hauck, C. (2019). Mountain permafrost degradation documented through a network of permanent electrical resistivity tomography sites. *The Cryosphere*, *13*(10), 2557–2578. https://doi.org/10.5194/tc-13-2557-2019

Monnier, S., Camerlynck, C., & Rejiba, F. (2008). Ground penetrating radar survey and stratigraphic interpretation of the Plan du Lac rock glaciers, Vanoise Massif, northern French Alps. *Permafrost and Periglacial Processes*, *19*(1), 19–30. https://doi.org/10.1002/ppp.610

Monnier, S., Camerlynck, C., & Rejiba, F. (2009). Ground-penetrating radar surveys on rock glaciers in the Vanoise Massif (Northern French Alps): Methodological issues. *Géomorphologie: Relief, Processus, Environnement*, *15*(2), 129–140. https://doi.org/10.4000/geomorphologie.7569

Müller, J., Vieli, A., & Gärtner-Roer, I. (2016). Rock glaciers on the run: Understanding rock glacier landform evolution and recent changes from numerical flow modeling. *The Cryosphere*, *10*(6), 2865–2886. https://doi.org/10.5194/tc-10-2865-2016

Naaim, M., Nicolas, E., Giraud, G., Faug, T., Chambon, G., Naaim, F., & Richard, D. (2016). Impact du réchauffement climatique sur l'activité avalancheuse et multiplication des avalanches humides dans les Alpes françaises. *La Houille Blanche*, *9*. https://doi.org/10.1051/lhb/2016055

Nuth, C., & Kääb, A. (2011). Co-registration and bias corrections of satellite elevation data sets for quantifying glacier thickness change. *The Cryosphere*, *5*(1), 271–290. https://doi.org/10.5194/tc-5-271-2011

Nye, J. F. (1965). The flow of a glacier in a channel of rectangular, elliptic or parabolic cross-section. *Journal of Glaciology*, *5*(41), 661–690. https://doi.org/10.3189/S0022143000018670

Oerlemans, J. (2005). Extracting a climate signal from 169 glacier records. *Science*, *308*(5722), 675–677. https://doi.org/10.1126/science.1107046

Olyphant, G. A. (1983). Computer simulation of rock-glacier development under viscous and pseudoplastic flow. *GSA Bulletin*, *94*(4), 499–505. https://doi.org/10.1130/0016-7606(1983)94<499:CSORDU>2.0.CO;2

Paul, F., Rastner, P., Azzoni, R. S., Diolaiuti, G., Fugazza, D., Le Bris, R., et al. (2020). Glacier shrinkage in the Alps continues unabated as revealed by a new glacier inventory from Sentinel-2. *Earth System Science Data*, *12*(3), 1805–1821. https://doi.org/10.5194/essd-12-1805-2020

PERMOS. (2016). Permafrost in Switzerland 2014/2015 to 2017/2018. https://doi.org/10.13093/permos-rep-2019-16-1

PERMOS. (2019). *Swiss permafrost monitoring network database (PERMOS database)*. Switzerland. Fribourg and Davos. https://doi.org/10.13093/permos-2019-01

Piermattei, L., Carturan, L., de Blasi, F., Tarolli, P., Dalla Fontana, G., Vettore, A., & Pfeifer, N. (2015). Analysis of glacial and periglacial processes using structure from motion. *Earth Surface Dynamics Discussions*, *3*, 1345–1398. https://doi.org/10.5194/esurfd-3-1345-2015

Plu, D., & Ducher, G. (1988). Availability of aerial photography and space images; the photothèque at the IGN (F), France. *Photogrammetria*, *43*(2), 83–100. https://doi.org/10.1016/0031-8663(88)90024-5

Pruessner, L. (2017). *Near-surface energy balance on an alpine rock glacier: Murtèl-Corvatsch*. Retrieved from http://urn.kb.se/resolve?urn=urn:nbn:se:uu:diva-323564

Ravanel, L., & Deline, P. (2011). Climate influence on rockfalls in high-Alpine steep rockwalls: The north side of the Aiguilles de Chamonix (Mont Blanc massif) since the end of the 'Little Ice Age'. *The Holocene*, *21*(2), 357–365. https://doi.org/10.1177/0959683610374887

Ravanel, L., Magnin, F., & Deline, P. (2017). Impacts of the 2003 and 2015 summer heatwaves on permafrost-affected rock-walls in the Mont Blanc massif. *The Science of the Total Environment*, *609*, 132–143. https://doi.org/10.1016/j.scitotenv.2017.07.055

Refsnider, K. A., & Brugger, K. A. (2007). Rock glaciers in Central Colorado, U.S.A., as indicators of holocene climate change. *Arctic Antarctic and Alpine Research*, *39*(1), 127–136. https://doi.org/10.1657/1523-0430(2007)39[127:RGICCU]2.0.CO;2

Reynolds, J. M. (2011). *An introduction to applied and environmental geophysics*. John Wiley & Sons. https://doi.org/10.1071/PVv2011n155other

Rodríguez, A., Mas, S., Richard, D., & Chirié, F. (2008). IGN Spain and IGN France collaboration to set up cross border INSPIRE compliant services, 10.

Scambos, T. A., Dutkiewicz, M. J., Wilson, J. C., & Bindschadler, R. A. (1992). Application of image cross-correlation to the measurement of glacier velocity using satellite image data. *Remote Sensing of Environment*, *42*(3), 177–186. https://doi.org/10.1016/0034-4257(92)90101-O

Schoeneich, P., Bodin, X., Echelard, T., Kaufmann, V., Kellerer-Pirklbauer, A., Krysiecki, J.-M., & Lieb, G. K. (2015). Velocity changes of rock glaciers and induced hazards. In G. Lollino, A. Manconi, J. Clague, W. Shan, & M. Chiarle (Eds.), *Engineering geology for society and territory* - (Vol. 1, pp. 223–227). Cham. Springer International Publishing. https://doi.org/10.1007/978-3-319-09300-0_42

SINTEGRA. (2012). Acquisition d'une couverture topographique par méthode Laser: Station Alpine Joseph Fourier - Jardin Botanique Alpin du Lautaret (Vol. 10330, p. 11). Rapport de campagne LiDAR.

Six, D., & Vincent, C. (2014). Sensitivity of mass balance and equilibrium-line altitude to climate change in the French Alps. *Journal of Glaciology*, *60*(223), 867–878. https://doi.org/10.3189/2014JoG14J014

Smith, M. W., Carrivick, J. L., & Quincey, D. J. (2015). Structure from motion photogrammetry in physical geography. *Progress in Physical Geography: Earth and Environment*, *40*(2), 247–275. https://doi.org/10.1177/0309133315615805

Sorg, A., Kääb, A., Roesch, A., Bigler, C., & Stoffel, M. (2015). Contrasting responses of Central Asian rock glaciers to global warming. *Scientific Reports*, *5*, 8228. https://doi.org/10.1038/srep08228

Springman, S. M., Arenson, L. U., Yamamoto, Y., Maurer, H., Kos, A., Buchli, T., & Derungs, G. (2012). Multidisciplinary investigations on three rock glaciers in the Swiss Alps: Legacies and future perspectives. *Geografiska Annaler - Series A: Physical Geography*, *94*(2), 215–243. https://doi.org/10.1111/j.1468-0459.2012.00464.x

Thibert, E., Blanc, R., Vincent, C., & Eckert, N. (2008). Glaciological and volumetric mass-balance measurements: Error analysis over 51 years for Glacier de Sarennes, French Alps. *Journal of Glaciology*, *54*(186), 522–532. https://doi.org/10.3189/002214308785837093

Thibert, E., Bonnefoy-Demongeot, M., Finance, F., Bodin, X. (2018) Extracting the time signal in surface velocity changes along 3 decades at Laurichard rock glacier (French Alps). In P. Deline, X. Bodin, & L. Ravanel (Eds.). *Proceeding of the 5th European conference on permafrost, 23 June–1 July 2018, Chamonix, France*. pp. 615–616.

Trabant, D. C., & Mayo, L. R. (1985). Estimation and effects of internal accumulation on five glaciers in Alaska. *Annals of Glaciology*, *6*, 113–117. https://doi.org/10.3189/1985AoG6-1-113-117

Trenberth, K. E., Jones, P. D., Ambenje, P., Bojariu, R., Easterling, D., Klein Tank, A., et al. (2007). Observations: Surface and atmospheric climate change. In Climate change 2007: The physical science basis. Contribution of Working Group I to the Fourth Assessment Report of the Intergovernmental Panel on Climate Change *Chapter 3*. United Kingdom. Retrieved from http://www.ipcc.ch/pdf/assessment-report/ar4/wg1/ar4-wg1-chapter3.pdf

Vernay, M., Lafaysse, M., Hagenmuller, P., Nheili, R., Verfaillie, D., & Morin, S. (2020). The S2M meteorological and snow cover reanalysis in the French mountainous areas (1958–present). [Data set]. AERIS. https://doi.org/10.25326/37

Vincent, C. (2002). Influence of climate change over the 20th Century on four French glacier mass balances. *Journal of Geophysical Research*, *107*(D19), 4375. https://doi.org/10.1029/2001JD000832

Vincent, C., Fischer, A., Mayer, C., Bauder, A., Galos, S. P., Funk, M., et al. (2017). Common climatic signal from glaciers in the European Alps over the last 50 years. *Geophysical Research Letters*, *44*, 1376–1383. https://doi.org/10.1002/2016GL072094

Wagner, S. (1992). Creep of alpine permafrost, investigated on the Murtel rock glacier. *Permafrost and Periglacial Processes*, *3*, 157–162. https://doi.org/10.1002/ppp.3430030214

Walter, F., Amann, F., Kos, A., Kenner, R., Phillips, M., de Preux, A., et al. (2020). Direct observations of a three million cubic meter rock-slope collapse with almost immediate initiation of ensuing debris flows. *Geomorphology*, *351*, 106933. https://doi.org/10.1016/j.geomorph.2019.106933

Whalley, B., & Azizi, F. (1994). Rheological models of active rock glaciers: Evaluation, critique and a possible test. *Permafrost and Periglacial Processes*, *5*, 37–51. https://doi.org/10.1002/ppp.3430050105

Wicky, J., & Hauck, C. (2020). Air convection in the active layer of rock glaciers. *Frontiers of Earth Science*, *8*. https://doi.org/10.3389/feart.2020.00335

Wirz, V., Geertsema, M., Gruber, S., & Purves, R. S. (2016). Temporal variability of diverse mountain permafrost slope movements derived from multi-year daily GPS data, Mattertal, Switzerland. *Landslides*, *13*(1), 67–83. https://doi.org/10.1007/s10346-014-0544-3

Zenklusen Mutter, E., & Phillips, M. (2011). Thermal evidence of recent talik formation in Ritigraben rock glacier: Swiss Alps. In *Proceedings of the 10th International Conference on Permafrost. Presented at the 10th International Conference on Permafrost, Salekhard, Russia*. Retrieved from https://www.dora.lib4ri.ch/wsl/islandora/object/wsl%3A20703